OPTIMIZATION OF SUPERLATTICES WITH CENTRAL QUANTUM WELL AND ALL-OPTICAL LOGIC GATES

LUIS EDUARDO PEDRAZA CABALLERO

OPTIMIZATION OF SUPERLATTICES WITH CENTRAL QUANTUM WELL AND ALL-OPTICAL LOGIC GATES

Dissertação apresentada ao Programa de Pós-Graduação em Ciência da Computação do Instituto de Ciências Exatas da Universidade Federal de Minas Gerais como requisito parcial para a obtenção do grau de Mestre em Ciência da Computação.

Orientador: Omar Paranaiba Vilela Neto

Belo Horizonte

Fevereiro de 2016

LUIS EDUARDO PEDRAZA CABALLERO

OPTIMIZATION OF SUPERLATTICES WITH CENTRAL QUANTUM WELL AND ALL-OPTICAL LOGIC GATES

Dissertation presented to the Graduate Program in Computer Science of the Universidade Federal de Minas Gerais in partial fulfillment of the requirements for the degree of Master in Computer Science.

ADVISOR: OMAR PARANAIBA VILELA NETO

Belo Horizonte

February 2016

UNIVERSIDADE FEDERAL DE MINAS GERAIS
INSTITUTO DE CIÊNCIAS EXATAS
PROGRAMA DE PÓS-GRADUAÇÃO EM CIÊNCIA DA COMPUTAÇÃO

FOLHA DE APROVAÇÃO

Optimization of Superlattices With Central Quantum Well and All-Optical
Logic Gates

LUIS EDUARDO PEDRAZA CABALLERO

Dissertação defendida e aprovada pela banca examinadora constituída pelos Senhores:

PROF. OMAR PARANAÍBA VILELA NETO - Orientador
Departamento de Ciência da Computação - UFMG

PROF. MARCOS AUGUSTO MENEZES VIEIRA
Departamento de Ciência da Computação - UFMG

PROF. PAULO SÉRGIO SOARES GUIMARÃES
Departamento de Física - UFMG

Belo Horizonte, 15 de fevereiro de 2016.

To the people that believed that this was possible.

Acknowledgments

To my family: Maria, Euclides, Leguis, Andres, Marian and Manuel for their support.

To my advisor: Omar Paranaiba, for giving me the opportunity to come from afar to achieve this step in my life. For his teachings, sincerity, critical view and friendship.

To my Brazilian brothers: Artur, Andre, Leandro, Thiago, Rafael, Clebson, Gabriel, Keiller, also called: Mitos do Cabral, for their sincere friendship.

To the people that are far away, but it seems they are here: Edinson, Jesus, Jorge, Julio, Johnathan, Virgilio.

To my professors Sonia and Darwin.

To my colleagues: Vinicius, Osvaldo, Alloma, Braulio, Iago.

To the Colombians in BH: Juan, Ricardo, Sergio, Andres, Diego, Jesus, Camilo, Lenka, Carolina, Adriana, Susana.

To Paulo Sergio, Juan Pablo and Marcello for their physical support to develop this work.

To my labmates: Jefferson, Luiz, Fernando, Bruno, Charles, Vitor, Lucas.

To the Brazilian government, particularly the CNPQ for the financial support.

Finally, to the people of the DCC.

"Three things you can't take back: a spent arrow, a spoken word and a lost opportunity."

(Arab proverb)

Resumo

Neste trabalho, dois estudos de casos que relacionam Ciências da Computação e Nanotecnologia são objeto de estudo, a través de duas recentes áreas de pesquisa: Nanotecnologia Computacional e Nanocomputação.

No primeiro caso, um algoritmo genético (GA) é utilizado para otimizar um tipo de estruturas conhecidas como superredes com poço quântico central. A otimização dessas estruturas é realizada variando a geometria que a compoe, com o intuito de encontrar sistemas que em sua configuração energética, os estados discretos de energia estejam o mais próximo possível do inicio das minibandas. Isto, dado o fato de que estruturas com essas particularidades apresentam alta capacidade de detecção e fotodetetores mais eficientes podem ser desenvolvidos. A variação geométrica consiste em modificar: o número de poços; largura do poço central, dos poços da superrede e das barreiras e altura das barreiras, o que gera inumeráveis configurações energéticas que são difíceis de prever. Desta forma, o processo de otimização se torna um dominio desconhecido, complexo e que demanda um amplo conhecimento de especialistas, por tanto, técnicas de otimização como os GAs são alternativas eficazes que podem auxiliar na solução deste tipo de problemas.

Os resultados obtidos mostram que o GA aplicado neste trabalho é uma tecnica adequada que se adaptou corretamente para o processo de otimização e as melhores estruturas descobertas apresentam características interessantes e grande potencial para serem sintetizadas experimentalmente.

No segundo caso de estudo, os cristais fotônicos são estudados para desenhar e projetar portas lógicas inteiramente óticas, visando o desenvolvimento de uma geração de computadores que opere com alta velocidade de procesamento de dados, baixo consumo energético e baixa dissipação de calor. Isto, motivado pelo fato de que os transistores baseados na tecnologia CMOS estão próximos do seu limite físico de miniaturização, além de que os dispositivos computacionais atuais, tem alto consumo energético e alta dissipação de energia em forma de calor.

Neste trabalho são utilizados as guias de onda em cristais fotônicos para contolar

o fenômeno de interferência de luz e desta forma projetar portas lógicas. Duas novas portas lógicas inteiramente óticas utilizando cristais fotônicos foram projetadas, a porta da Maioria e a porta de Feyman. A primeira é muito importante para o desenvolvimento de circuitos otimizados e simplificados, a segunda é uma porta reversível que permite a criação de circuitos no limite mínimo de consumo energético. Adicionalmente, foi aplicada uma metodologia para analisar a robustez destes dispositivos com o objetivo de avaliar a tolerância às falhas ante possíveis erros no processo de crescimento físico. Os resultados obtidos mostram que os dispositivos projetados com essa abordagem são robustos e têm a capacidade de suportar grandes erros no processo de síntese com 95% de confiança.

Palavras-chave: Nanodispositivos Semicondutores, Superredes com Poço Quântico Central, Algoritmo Genético, Cristais Fotônicos, Portas Logicas Fotônicas, Análise de Robustez..

Abstract

In this work, two study cases linking Computer Science and Nanotechnology are studied, through two recent research areas: Computational Nanotechnology and Nanocomputing.

In the first case, a genetic algorithm (GA) is applied to optimize one type of structures known as superlattices with central quantum well. The optimization of these structures is accomplished varying the geometry that compose it, aiming to find systems in that their energetic configuration, the discrete energy levels must close of the beginning of the minibands. This, due to the that structures with these features exhibit high capacity detection and efficient photodetectors can be development. The geometrical variation consist in modify: the number of quantum wells; width of the central well, wells of the supperlattice and the barriers and hight of the barriers, generating countless energetic configurations difficult to predict. Consequently, the optimization process becomes a unknown domain, complex and demanding extensive knowledge and intuition of experts, then, optimization techniques such as GAs are effective alternatives to aid in the solution of these problems.

The results obtained here show that the GA is an adequate techniques for the optimization of this kind of structures and the better structures discovery present interesting features and great potential to be synthesized experimentally.

In the second study case, photonic crystals are studied to design and project all-optical logic gates, aiming the development of a computers generation operating with high data processing speed, low power consumption and low dissipation of energy. This, motivated by the reason that the transistor based on CMOS technology is close to its physical limit of miniaturization as a result of various effects that are not found at larger scales, such as current leakage. Also, the computational devices today have high power consumption and dissipation of energy to heat.

In this project, photonic crystals waveguides are used to control the light beam interference effect focusing in the design of all-optical logic gates. Two new logic devices in photonic crystals were proposed in this work, the Majority and Feynman gates. The

former is very important to develop simplified and optimized circuits, the latter is a reversible logic gate that allows the creation of computational circuits in the minimum limit of energy consumption. Additionally, a methodology to analyse the robustness of these devices is applied with the goal to evaluate the fault tolerance in the physical growth. The results obtained show that the devices projected with this approach are robust and have the capacity to tolerate high disorders in the physical growth process with 95 % of confidence level.

Palavras-chave: Semiconductors nanodevices, Superlattices With Central Quantum Well, Genetic Algorithm, Photonic Crystals, Photonic Logic Gates, Robustness Analysis.

List of Figures

List of Tables

Contents

List of Acronyms

Acronym	Description
CQW	Central Quantum Well
GA	Genetic Algorithm
Phc	Photonic Crystal
SPQW	Superlattice of Quantum Wells

Chapter 1

Introduction

1.1 Motivation

In recent years, two research areas that link computer science and nanotechnology have been gaining ground. These are: computational nanotechnology and nanocomputing.

The first focusses on the application of computational tools and algorithms to support the evolution of the nanoscience and nanotechnology, specifically to develop and discover new materials and devices at the nano scale. On the other hand, nanocomputing investigates materials and devices at nano scale as alternatives technologies to develop new generations of computers with low power consumption and high data processing speed.

In this work, two study cases related with computational nanotechnology and nanocomputing are investigated.

The first motivated by the difficulty found by scientists to optimize one kind of quantum structures known as superlattices with central quantum well (SPQW). These are periodic structures formed by the repetition of quantum wells with thin barriers separating them and a quantum central well. Consequently, discrete energy states and minibands are present in their energy-band configuration. Modifications in the geometry of it, such as: number of quantum wells, width of quantum wells and barriers, height of the barriers, cause different energy-band configurations.

The localization of the discrete energy states and minibands in SPQW is accomplished through a visual observation by an expert, demanding extensive knowledge and intuition. In addition, finding structures with specific energy-band configuration is a hard, empirical and slow optimization process.

For this reason, the use of robust, effective and efficient computational techniques and optimization algorithms to support this process is necessary. Thus, a genetic al-

gorithm is an adequate optimization approach to find SPQW structures with desired energy-band configuration in order to develop new optoelectronic devices such as photodetectors.

The second study case is inspired by the reason that the silicon transistor is close to its physical limit of miniaturization as a result of various effects that are not found at larger scales, such as current leakage. Consequently, smaller computers with greater data processing speed and high capacity of data storage might not be developed. Also, the computational devices today have high power consumption and dissipation of energy to heat. Then, it is necessary to explore new materials and technologies to find the successor of silicon transistor.

One possible alternative is the optical technology. In this, the information processing is realized using all-optical devices. For optical technology is expected considerable reduction of dissipation, low power consumption and high speed of data processing.

In this way, photonic crystals are materials with low absorption and periodic refractive indices. The periodicity can be in one, two or three dimensions. Two dimensional photonic crystals can be designed to create a complete photonic band gap, preventing light from propagating in certain directions with specified frequencies. This phenomena is used to create a photonic crystal waveguide. A waveguide is a controlled defect in the crystal, able to guide the light in desired directions of propagation, Joannopoulos et al. [2008]. Then, a photonic crystal waveguide is a perfect platform to design all-optical logic devices aiming the creation of photonic integrated circuits.

1.2   Goals

For the superlattice with central quantum well optimization, the goal is to find structures with a desired energy-band configuration through a genetic algorithm by varying the geometry parameters that compose them. This, aiming to develop and discover new optoelectronic devices such as photodetectors with high detection capacity. The parameters to be modified are: number of quantum wells, width of the central quantum well, width of the quantum wells that form the superlattice, width of the barriers and height of the barriers.

In the work with photonic crystals, the goal is to project new all-optical logic gates controlling the light beam interference effect through the photonic crystals waveguide. Additionally, a methodology for the robustness analysis of all-optical logic devices in photonic crystals will be performed to evaluate the fault tolerance of these devices. This, focusing on the development of a new generation of computers that operate with

low power consumption and high speed of data processing.

1.3 Contributions

The main contributions of this project are: for the superlattices with central quantum well optimization, an approximated method was developed to achieve automatically the energy-band configuration of these structures. This method in conjunction with a genetic algorithm are applied to find superlattices of quantum wells with desired energy states. The best structures found in this work have great potential to be grown experimentally in order to develop optoelectronic devices such as photodetectors.

In the work with photonic crystals, two all-optical logic gates were projected using the light beam interference effect. These are: the Majority and Feynman gates. The first is very important to develop simplified and optimized circuits, the second is a reversible logic gate that allows the creation of circuits in the minimum limit of energetic consumption. Additionally, a robustness analysis methodology was proposed and demonstrated that the all-optical logic devices designed with photonic crystals waveguide are robust and can tolerate high errors in the growth physical process.

1.4 Roadmap

This manuscript is organized as follows: Chapter 2 presents an overview of semiconductors, superlattices of quantum wells and photonic crystals. Chapter 3 discusses the main works in optimization of nanostructures and nanodevices, also, the recent works with all-optical logic gates using photonic crystals. Chapter 4 describes the optimization process and the simulation results of the superlattice of quantum wells structures. In Chapter 5 are presented the all-optical logic gates proposed here and the robustness analysis of logic devices. Finally, Chapter 6 gathers the main conclusions and the future work.

Chapter 2

Background

Nanocomputing and Computational Nanotechnology are two recent research areas linking Computer Science and Nanotechnology, so, in order to better understand this work, this section gives an introduction to what Semiconductors, Superlattices of Quantum Wells Structures, Photonic Crystals and Genetic Algorithms are, and how they work.

2.1   Semiconductors

In solid state physics, crystals are defined as periodic arrangements of atoms or molecules characterized by a crystal lattice, which has the geometrical information of the periodic pattern. Consequently, an atomic crystal determines a periodic potential which produces fascinating consequences in the electron transport throughout the crystal, and characterizes the electric properties of the material, Rezende [2004].

Electrons suffer scattering in crystals when the size of the scatterers (atoms or molecules) are of the order of the De Broglie wavelength, giving rise to interference phenomena between the multiple scattered electron waves. Such interference can be constructive, determining allowed states known as bands, e.g., valence and conduction bands; or destructive, determining forbidden states known as band gaps. Each crystal has its own energy-band configuration. Thus, there are several possible energy-band conditions to consider, Neamen [2003].

First, when the material is an insulator, the last energy band with electrons is completely filled with electrons. Then, if an electric field is applied, there are no particles to move, so there will be no current, as shown in Figure 2.1a, Neamen [2003].

In the second case, the crystal has the characteristics of a conductor, exhibiting a very high electrical conductivity. For this condition, the last energy band with electrons
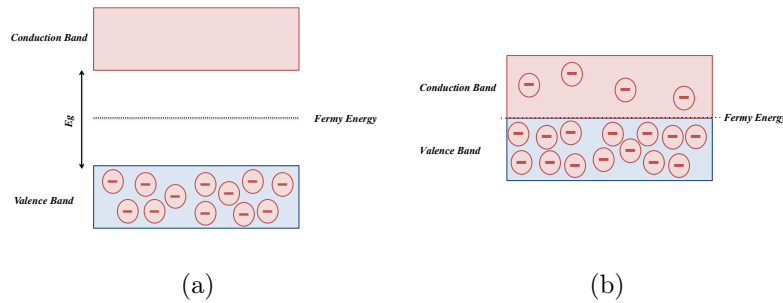
Figure 2.1: Energy band configuration for (a) Insulator and (b) Conductor

is not completely filled, so an electric field can put electrons in movement, thus, allowing conduction, as illustrated in Figure 2.1b, Neamen [2003].

Finally, when the material is a semiconductor, the last energy band of a crystal is completely filled, only at temperature $T = 0$ K. When the temperature is higher than zero, valence band electrons can gain enough thermal energy to reach the next band, called conduction band, which was empty at $T = 0$. The migration of electrons to the conduction band leaves, in the valence band, states that behave such as positive charge carriers, called holes. The electrons in the conduction band and holes in the valence band produce electrical current under the action of an external field. The conductivity of the material depends on the number of electrons that passes into the conduction band, which can be calculated probabilistically. This amount of electrons is proportional to the temperature and the inverse of the energy gap between the two bands. This energy is represented by Eg, where g is the gap index. The materials which are insulators at $T = 0$ K, but have an Eg relatively small, on the order of 1 eV or less at room temperature, have significant conductivity and, therefore, are called semiconductors. Figure 2.2 shows the occupation of the valence and conduction bands in a semiconductor.

In these materials, the number of electrons in the conduction band can be higher in relation to an insulator, but it is still much less than the number of free electrons in a metal. Therefore, the conductivity of the semiconductor is much smaller than that of metals. The main difference between an insulator and a semiconductor is the value of Eg. For example, silicon has $Eg = 1.1$ eV and is a semiconductor, while diamond which has the same structure of Silicon (Si), but comprised of atoms of Carbon (C) has $Eg = 5$ eV, and behaves as a good insulator. The Silicon Oxide, SiO_2, has an $Eg \simeq 8$ eV and is also an insulator. The difference in the values of Eg may not seem so great to produce radical change in conductivity, however, the occupation of the

(a)   (b)
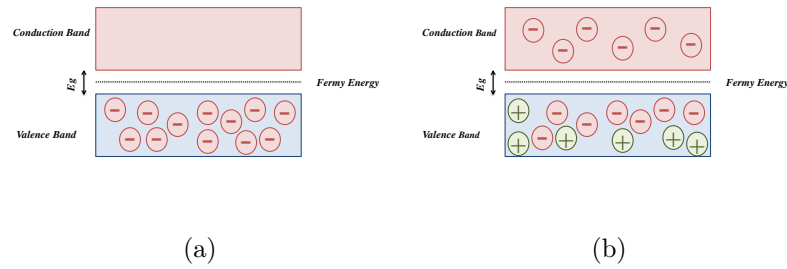
Figure 2.2: Energy band configuration for (a) Semiconductor at $T = 0K$ and (b) Semiconductor at $T > 0K$

conduction band decreases exponentially with the increase of the $\frac{E_g}{k_B T}$ ratio, where k_B is the Boltzmann constant, as described in Rezende [2004].

2.2 Superlattice of Quantum Wells

A semiconductor quantum well is a sandwich structure, in which a piece of narrow-gap material (well) is placed between two pieces of wider-gap material (barriers), as shown in Figure 2.3. This is a kind of quantum-confined structure in which the motion of the electrons (and/or holes) are confined in one directions by the potential barriers, Duan and Guojun [2005].

The quantum confinement is provided by the discontinuity in the band gap at the interfaces, which leads to a spatial variation of the conduction and valence bands, as shown in the lower half of the Figure 2.3.
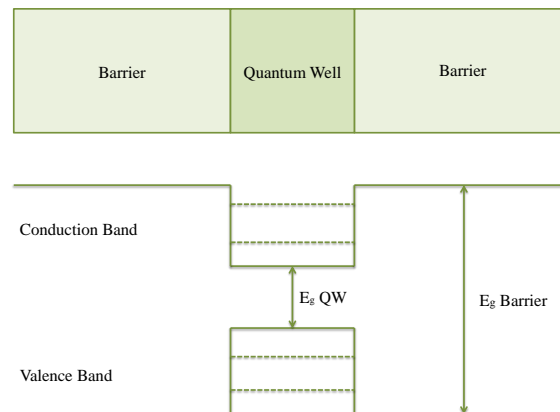
Figure 2.3: Quantum Well Structure. Dashed lines represent discrete energy levels.

Thus, the motion of the electrons and holes will be quantized in the growth (z) direction, giving rise to a series of discrete energy levels, as indicated by the dashed lines inside the quantum well in Figure 2.3. The motion in the other two directions (i. e. the x-y plane) is still free, and so we have quasi two-dimensional (2-D) behaviour, Kasap and Capper [2007].

A superlattice of quantum wells structure consists of many repeated quantum wells with thin barriers separating them, as illustrated in Figure 2.4. Superlattices behave like artificial one-dimensional periodic crystals, in which the periodicity is designed into the structure by the repetition of the quantum wells. The electronic states of superlattices form delocalised minibands as the wave functions in neighbouring wells couple together through the thin barrier that separates them, Kasap and Capper [2007].
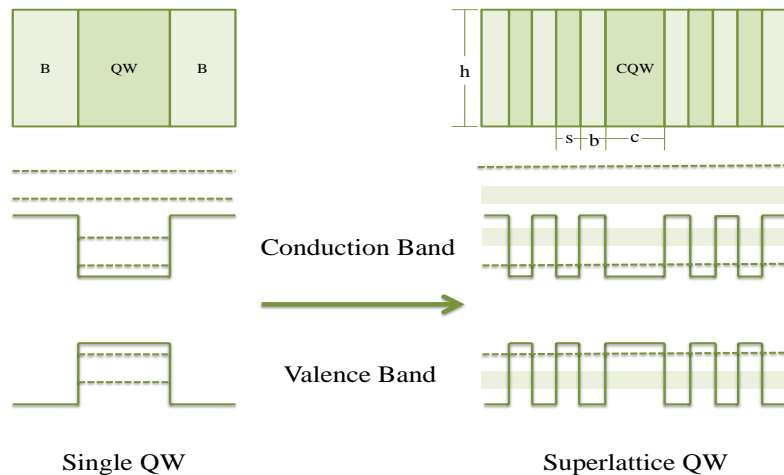
Figure 2.4: Superlattice of Quantum Wells Structure. Dashed lines represents discrete energy levels and the shaded areas minibands.

Quantum wells and superlattices of quantum wells structures in general have many uses. They can be used for advanced electronic devices (e.g., modulation-doped field-effect transistors, heterojunction bipolar transistors, resonant tunneling devices), optical components (e.g., waveguides, mirrors, fiber-optic communication, laser printing, compact disc, CD-ROM, scientific instruments), and optoelectronic devices and structures (e.g., laser diodes, photodetectors, optoelectronic devices). Although heterostructures may be useful in electronics, they are crucial in many optoelectronic devices. Perhaps, their most important technological aspect may be that they can be used for all of these electronic, optical, and optoelectronic purposes, and hence may allow the integration of all of these, Gossard et al. [2000].

2.3   Photonic Crystals

The optical analogue of an atomic crystal semiconductor is known as a photonic crystal, which is a material whose dielectric function is periodic and they are described by an underlying crystal lattice. As electrons in periodic potential, electromagnetic waves in a photonic crystal undergo scattering when their wavelengths are of the order of the size of the dielectrics forming the crystal, Joannopoulos et al. [2008].

Photonic bands (allowed states) arise as a consequence of constructive interference phenomena, and photonic band gaps arise as a consequence of destructive interference phenomena. Defects in the periodic structure can be introduced in a photonic crystal and they can induce the localization of the electromagnetic field around the defect, and these localized states can have associated frequencies inside the photonic band gap region. Photonic crystals can be periodic in one, two or three dimensions, each of these offering particular functionalities and applications, Joannopoulos et al. [2008].

Two dimensional photonic crystals, as shown in Figure 2.5, can be designed to create a complete photonic band gap, preventing light from propagating in certain directions with specified frequencies (i.e., within a certain range of wavelengths of light colors).
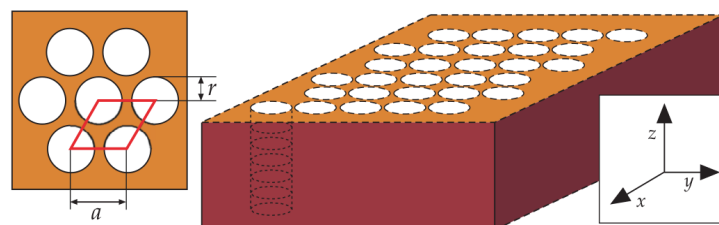
Figure 2.5: Two dimensional photonic crystal. Taken from Joannopoulos et al. [2008].

In particular, there are two types of defects that can be introduced in two-dimensional photonic crystals: point defects and line defects. The former are known as cavities, illustrated in Figure 2.6, and the latter as waveguides, as shown in Figure 2.7.

Cavities in photonic crystals are used to localize the electromagnetic radiation, usually in a small volume with very small losses. On the other hand, waveguides are used to guide the electromagnetic radiation with very high efficiency, as shown in Figure 2.7b. One of the big advantages of photonic crystal cavities and waveguides is that electromagnetic waves at optical frequencies are only weakly absorbed by dielectric materials, different from metallic materials where the absorption at these frequencies
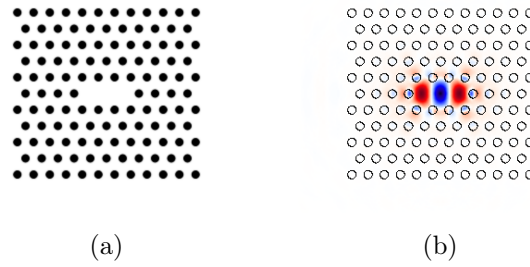
Figure 2.6: Photonic Crystal Cavity. (a) Dielectric distribution of the structure and (b) Electric field distribution.

is usually high. In this way, photonic crystals allow optical devices working in the low losses and low energy-consumption regime, Joannopoulos et al. [2008].
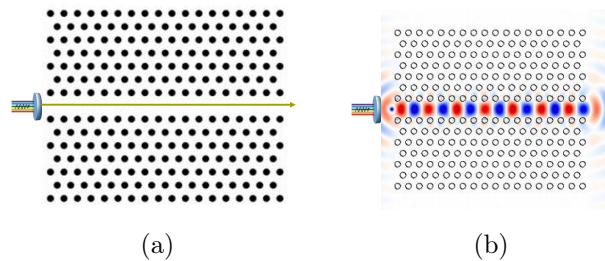
Figure 2.7: Photonic Crystal Waveguide. (a) Dielectric distribution of the structure and (b) Electric field distribution.

Photonic crystals have become very promising systems to achieve the desired all-optical information processing in photonic circuits. In particular, cavities and waveguides embedded in photonic materials can be used to design efficient all-optical computational devices with flexible functionalities.

2.4   Genetic Algorithm

Computational Intelligence is a branch of Computer Science that uses algorithms and techniques that mimic some cognitive abilities such as recognition, learning and development, to create programs, somehow intelligent. The best-known and used algorithms are: Genetic Algorithm, Artificial Neural Networks and Fuzzy Logic, Neto [2014].

Essentially, Genetic Algorithms are search and optimization methods, highly parallel, inspired by the principles of Darwinian natural selection and genetic reproduction,

which favor the fittest individuals living longer and therefore more likely to reproduce. Typically, the GAs operate as explained in Algorithm 1, Mitchell [1998].

Algorithm 1 Genetic Algorithm

1: **procedure** GA($Fitness$, n, p, r, m)
2:     $Fitness$: A function that assigns an evaluation score, given a hypothesis.
3:     n: The number of generations.
4:     p: The number of hypotheses to be included in the population.
5:     r: The fraction of the population to be replaced by Crossover at each step.
6:     m: The mutation rate.
7:     Initialize population: $P \leftarrow$ Generate p hypotheses at random.
8:     Evaluate: For each h in P, compute $Fitness(h)$.
9:     **while** Stop condition is not satisfied **do**
10:         Create a new generation, P_s:
11:         Select: Probabilistically select $(1 - r)p$ members of P to add to P_s.
12:         Crossover: Probabilistically select pair of hypotheses from P.
                For each pair, (h_1, h_2) , produce two offspring by applying the
                crossover operator.
                Add all offspring to P_s.
13:         Mutate: Choose m percent of the members of P, with uniform probability.
                For each, invert one randomly selected bit in its representation.
14:         Update: $P \leftarrow P_s$.
15:         Evaluate: for each h in P, compute $Fitness(h)$.
16:         speed $\leftarrow$ computeSpeed(
                gpx.track(i).segment(j).delta_s(q),
                gpx.track(i).segment(j).delta_t(q));
17:     **end while**
18:     Return the hypothesis from P that has the best fitness.
19: **end procedure**

These algorithms are inspired by the genetic processes of biological organisms to search for optimal solutions. To do so, it proceeds as follows: each potential solution to a problem can be encoded in a structure called chromosome, which consists of a string of bits or symbols, Michalewicz [2013]. So these chromosomes represent individuals that are evolved over several generations, similar to living beings, according to the principles of natural selection and survival of the fittest, as described by Darwin [1859]. Simulating these processes, Genetic Algorithms are able to evolve solutions to real world problems.

The evolution process starts with the creation of random individuals (solutions) that will form the initial population. From a selection process based on the fitness of each individual, individuals are chosen for reproduction phase, which creates new solutions using for this a set of genetic operators (crossover and mutation basically).

These new solutions will be evaluated and their skills will determine your probability of staying in subsequent generations, Golberg [1989].

The stop condition of the algorithm can be determined in several ways: the number of generations, the number of individuals created, getting a given evaluation value, i.e., an optimum, the processing time, and the degree of similarity among individuals in a population (indicating convergence).

Chapter 3

Related Work

3.1 Semiconductor Nanodevices Optimization

Computational Nanotechnology (or Computational Nanoscience) focuses in the application and development of algorithms and computational systems to aid the advances of nanoscience and nanotechnology. In this scenario, many computational techniques have been applied to support several studies researching the development and discovery of new materials and devices in the nano-scale.

In a work developed by Singulani et al. [2008] two computational intelligence techniques were applied, namely, Artificial Neural Network (ANN) and Genetic Algorithm to the growth of self-assembled quantum dots. The ANN was used to associate the growth input parameters with the mean height of the deposited quantum dots. The six different growth parameters used as input to create the ANN are: the indium flux in the reactor, the growth temperature, the deposition time, the width of the layer on top of which the dots are nucleated, the aluminum and indium contents of this layer material. Once the Neural Network was created, validated and tested, it has combined with the GA, enabling us to obtain the growth parameters which are, in principle, most suitable for minimizing the quantum dot mean height. This is accomplished by using an ANN to infer the behavior of the quantum dots, and after that, the GA technique to obtain the parameters configuration which leads to the minimum quantum dot mean height possible, given the growth parameters ranges used as input to the ANN.

Passaro et al. [2010] present a self-consistent optimization of multi-quantum well based nanostructured semiconductors. Two study cases are evaluated, to known: symmetric MQW of three wells with a larger one in the middle and MQW of ten wells and electric contacts. A Genetic Algorithm is used for the search module, based on the solution of the coupled Schrödinger and Poisson equation.

15

In another work, Deb et al. [2010] applied Genetic Algorithm (GA) and particle swarm optimization (PSO) techniques to determine the optimized system parameters for modulation doped $Al_xGa_{1-x}As/GaAs$ quantum well nanostructures. Electrical characteristics of carrier in quantum well are controlled by system parameters like quantum well width, spacer layer thickness, doping concentration, lattice temperature, external dc biasing field and frequency of applied ac field. All these parameters are related in such a way that it is very difficult to predict optimized parameter values for desired electrical characteristics. Optimized parameters computed with both techniques are analyzed to predict the flexibility in terms of parameters which may be utilized during the fabrication of better nanodevices. The authors showed that PSO achieved slightly better results.

Cotta et al. [2014] use a genetic algorithm for the the first quantitative study of parameters optimization for semiconductor microcavities synthesis under uncertainty. In this, optimal parameter set (aluminum concentrations x, thickness and the number of the layers) were found based on the reflectance spectra of a $Al_xGa_{1-x}As$ semiconductor microcavity. These parameters may offer increased robustness in the growth process, while providing a considerable Quality Factor and the desired position of the cavity resonance.

Also, evolutionary optimization has been used by Feichtner et al. [2012], to find improved nanoantenna structures and Chen et al. [2007] optimized the focusing quality of integrally gated Carbon Nanotube (CNT) field emission devices by numerical methods that include GAs. Ginzburg et al. [2011] presented a method for designing plasmonic particles with desired resonance spectra by exploiting the interaction of local geometry with surface charge distribution and applying an evolutionary algorithm. Forestiere et al. [2010] used GAs to design metal nanoparticle arrays that produce broadband plasmonic field enhancement over the entire visible spectral range.

In this project a genetic algorithm is applied to find superlattices of quantum wells structures restricted to a condition on their energy-band configuration. This condition dictates that the discrete energy levels must be close to the beginning of the minibands, because the detection capacity of the device increases. To achieve this, variations in the geometry of the structure are performed through the GA in order to produce different energy-band configurations. The geometry parameters altered are: number of quantum wells, width of the quantum central well, width of the quantum wells forming the superlattice, width and height of the barriers.

3.2   All-Optical Logic Gates

The first step for development of photonic computational circuits is the design and creation of all-optical logic gates. Recently, many schemes have been proposed to realize all-optical logic gates.

Rani et al. [2013] report an AND optical logic gate, shown in Figure 3.1, based on two dimensional triangular lattice of air holes in Si. The design of the structure consists of Y-branch waveguide without nonlinear materials and optical amplifiers. A point defect was inserted in the central rod of the structure to decrease the output power, when one of the inputs is set in 1. When both inputs are 1, the output power was increased so that a high transmission is obtained and an AND gate is accomplished.
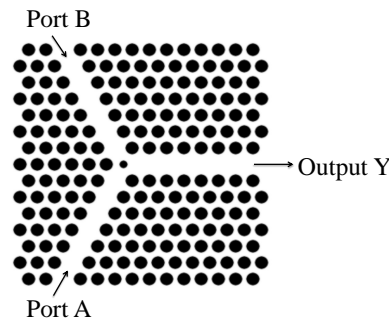
Figure 3.1: Schematic structure for AND logic gate proposed by Rani et al. [2013].

In another recent work, Yang et al. [2013] propose an all-optical AND gate based on a two-dimensional photonic crystal, illustrated in Figure 3.2. The device is composed of a ring resonator waveguide with two input-port waveguides and one output-port waveguide in triangular-lattice photonic crystals. The logic AND gate proposed can operate at various wavelengths such as 1.30, 1.43, 1.45, 1.49, 1.51, and 1.55 μm, considering the definitions of logic 0 and 1 being less than 35% and more than 95%, respectively.

All-optical logic gates, including OR, XOR, NOT, XNOR, and NAND gates, are realized theoretically by Fu et al. [2013] in a two-dimensional silicon photonic crystal using the light beam interference effect. The ingenious photonic crystal waveguide component design, the precisely controlled optical path difference, and the elaborate device configuration ensure the simultaneous realization of five types of logic gate with low-power and a contrast ratio between the logic states of 1 and 0 as high as 20 dB. High power is not necessary for operation of these logic gate devices. As shown in Figure 3.3, the schematic structure for the logic devices offers a simple and effective approach for the realization all-optical logic gates.
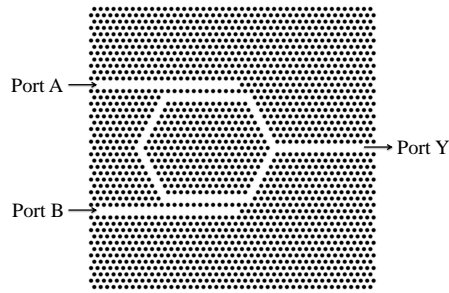
Figure 3.2: Schematic structure for AND logic gate proposed by Yang et al. [2013].
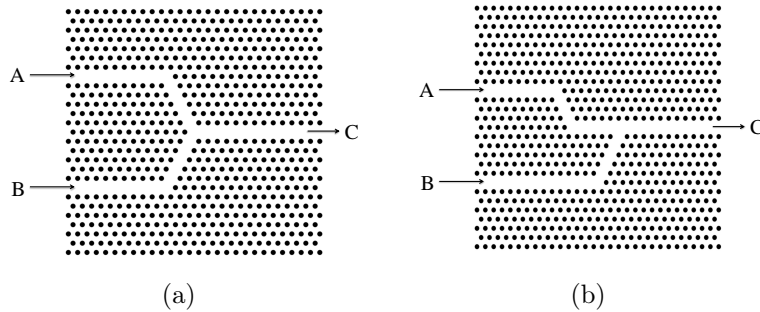
Figure 3.3: Schematic structure for the (a) OR and (b) XOR logic gates proposed by Fu et al. [2013].

Younis et al. [2014] propose two novel designs of compact, linear, and all-optical OR and AND logic gates based on photonic crystal architecture. The proposed devices are formed by the combination of the ring cavities and *Y-shape* line defect coupler placed between two waveguides. The suggested design for AND gate offers ON to OFF logic level contrast ratio of not less than 6 *dB* and the suggested design for OR gate offers transmitted power of not less than 0.5. On top of that, the proposed OR and AND logic gates can operate at bit rates of around 0.5 and 0.208 *Tb/s*, respectively. Further, the calculated fabrication tolerances of the suggested devices show that the rods radii of the ring cavities need to be controlled with no more than $\pm 10\%$ and $\pm 3\%$ fabrication errors for optical OR and AND gates, respectively. The schematic structure of these all-optical logic gates is shown in the Figure 3.4

More recent, Goudarzi et al. [2016] proposed an all-optical logic gate structure based on line and point defects created in the two dimensional square lattice of silicon rods in air photonic crystals (PhCs), shown in Figure 3.5. Line defects are embedded in the ΓX and ΓY directions of the momentum space. The device has two input and two output ports. It has been shown analytically whether the initial phase difference

(a)   (b)
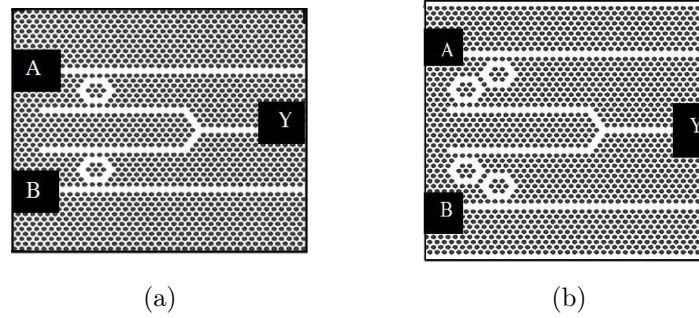
Figure 3.4: Schematic structure for the (a) OR and (b) AND logic gates proposed by Younis et al. [2014].

between the two input beams is $\frac{\pi}{2}$, they interfere together constructively or destructively to realize the logical functions. The authors reported that the device can acts as an *XOR* and an *OR* logic gate. The frequency operation range of the device is 0 to 0.45 $\left(\frac{a}{\lambda}\right)$, this ratio was set 0.419 for low dispersion condition, correspondingly the lambda is equal to 1.55 μm. The maximum delay time to response to the input signals is about 0.4 ps, hence the speed of the device is about 2.5 THz. Also 6.767 dB is the maximum contrast ratio of the device.
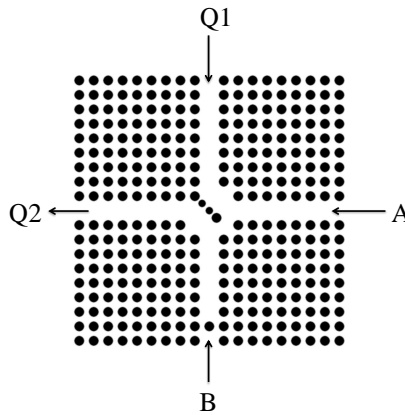
Figure 3.5: Schematic structure proposed by Goudarzi et al. [2016]. The output in Q1 is the XOR function and in Q2 is the OR function.

In this work, two new optical logic gates are proposed: the Majority gate and the Feynman gate. The former allows the creation of simple and optimized computational circuits and the latter is a reversible logic device projected to design circuits in the thermodynamic limit of computation. Additionally, a robustness analysis methodology is applied to evaluate the performance and fault tolerance of these devices.

Chapter 4

Optimization of Superlattices With Central Quantum Well

This chapter presents the methodology to apply the genetic algorithm, the problem definition, the optimization model and the simulation results of the optimization of the superlattices with central quantum well.

4.1 Problem Definition

4.1.1 Superlattice With Central Quantum Well Structures Desired

The design and search of superlattices of quantum wells with desired energy-band configuration behaviour is a very difficult process. However, this is an important step for the development and discovery of new optoelectronic devices.

The structures of our interest are geometrically composed by a central quantum well, n quantum wells to the left and right of the CQW and $(2*(n+1))$ barriers, see Figure 4.1. Modifications in the geometry of the structure produce different energy-band configuration, i.e, variations in the number of quantum wells, the width of the central quantum well, width of the quantum wells forming the superlattice, width and height of the barriers, are responsible for these effects.

The target here is to find structures restricted to the following condition:

The discrete energy levels must be close of the beginning of the minibands in the energy-band configuration of the structure, as illustrated in the Figure 4.2a. The main reason is that when an electric field is applied on the structure, the discrete energy level comes into the miniband, increasing the detection capacity of a photodetector.
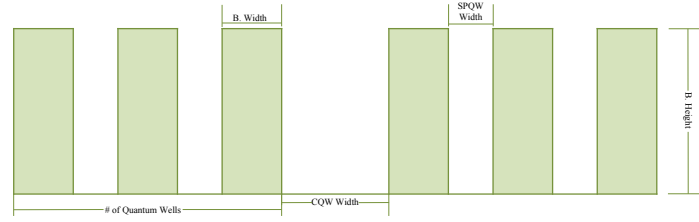
Figure 4.1: Superlattice of quantum wells geometry.
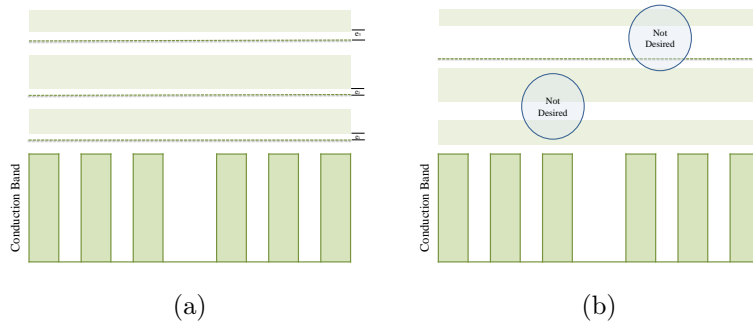
Figure 4.2: Example of a energy-band configuration desired (a) and not desidred (b).

In this project, only the discrete energy levels and minibands of the structure with energy above the barriers are investigated. The upper boundary of energy to be considered is 1600 meV, being the energy range of interest.

4.1.2   Detection of Energy States

As detailed in Section 2.2, a superlattice with central quantum well, like the one depicted in Figure 4.1, generates discrete energy levels and minibands.

Consider the structure with the parameters displayed in Table 4.1 and illustrated in Figure 4.3.

Number of Quantum Wells	5
Central Quantum Well Width	70 Ang.
Superlattices of Quantum Wells Width	20 Ang.
Barriers Width	70 Ang.
Barriers Height	500 meV

Table 4.1: Parameters of superlattice of quantum wells structure.

The first step to achieve the energy-band configurations of this kind of structures is to calculate and plot the transmission coefficient using the method described in
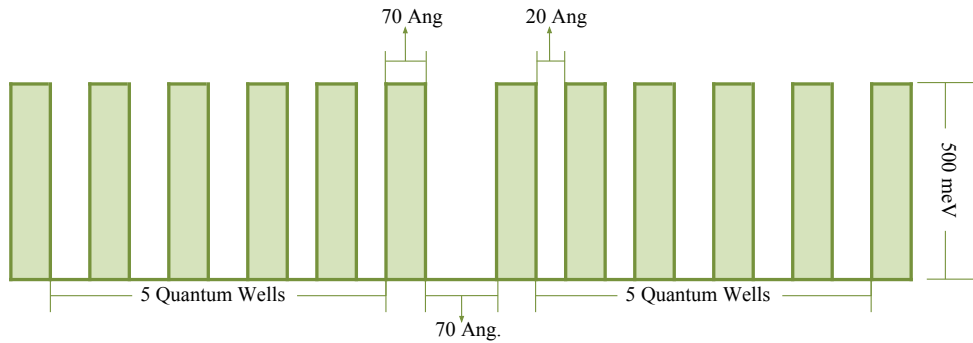
Figure 4.3: Superlattice of quantum wells structure example.

Degani and Maialle [2010]. After this, a visual observation by an expert is made to localize the discrete energy levels and minibands using the transmission plot. Figure 4.4 shows the transmission plot of the superlattice of quantum wells example. The discrete energy levels (in red), and the minibands (the regions inside the green rectangles) are shown.
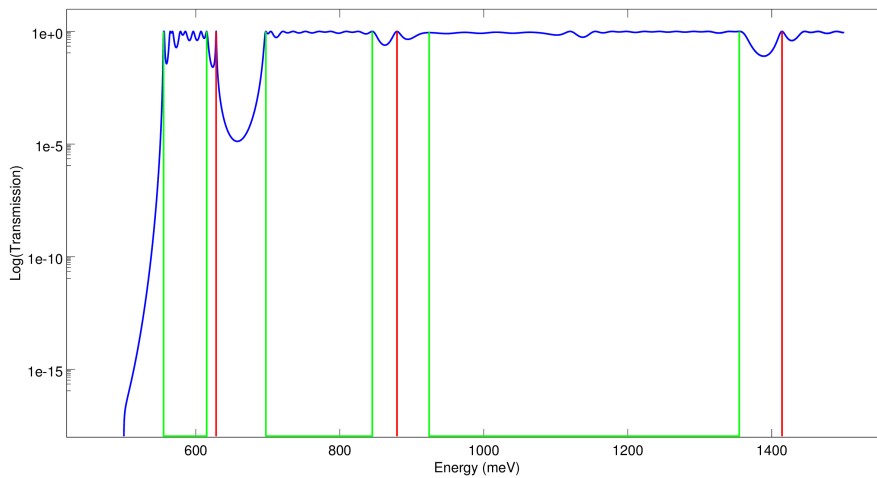
Figure 4.4: Transmission of superlattice of quantum wells structure example.

Obviously, this task is empirical, prone to errors and slow, demanding an extensive knowledge and intuition of experts.

For this reason, an approximate method to accomplish automatically the energy-band configuration of the superlattices of quantum wells was developed and implemented, as described below.

Firstly, the energy points of the maxima in the transmission coefficient are obtained and the wave function is recalculated for each point. Also, the square module

of the wave function is computed in the quantum wells of the superlattice and in the central quantum well, see Figure 4.5, to verify its localization, according to:

$$P_{SR} = \int\limits_{Superlattice} \mid \psi(x) \mid^2 dx \qquad (4.1)$$

$$P_{CQW} = \int\limits_{CQW} \mid \psi(x) \mid^2 dx \qquad (4.2)$$

where P_{SR} and P_{CQW} are the square modules of the wave function, $\psi(x)$, in the superlattice and in the central quantum well, respectively.
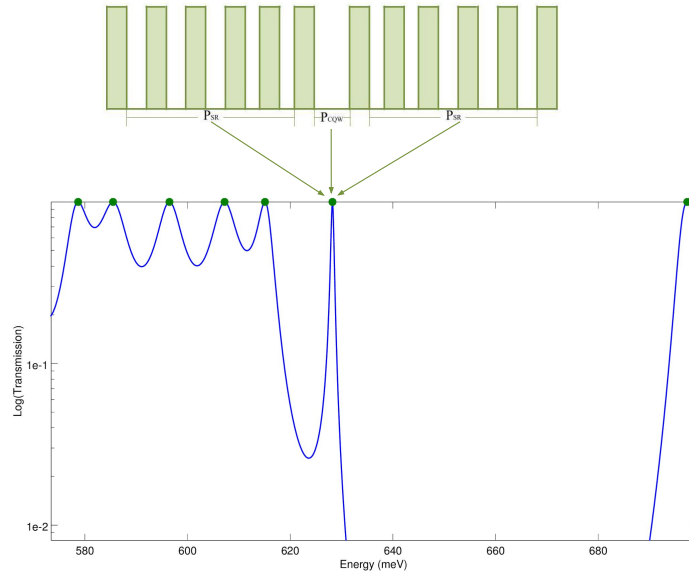
Figure 4.5: Localization of the wave function.

Once this is done, the ratio $r = \frac{P_{CQW}}{P_{SR}}$ is calculated. Note that when the wave function is localized closer to the quantum central well, r has a greater value than that when localized in the superlattice, therefore, the maximum point can be considered as a discrete energy level.

Finally, the mean and the standard deviation are computed, and the following factor is calculated:

$$f = \mu + \lambda\sigma \qquad (4.3)$$

where μ is the mean, λ is an empirical parameter and σ is the standard deviation. At this instance, if the r ratio of a maximum energy point is greater than the factor f, this point is considered a discrete energy level, otherwise is part of a miniband. Figure

4.6a shows the simulation result of the above procedure. Each point represents the ratio of the maximum points, red line the mean and the blue line the factor f. Figure 4.6b illustrates the energy-band configuration with the localized energy levels and the transmission coefficient of the SPQW example.

(a)

(b)
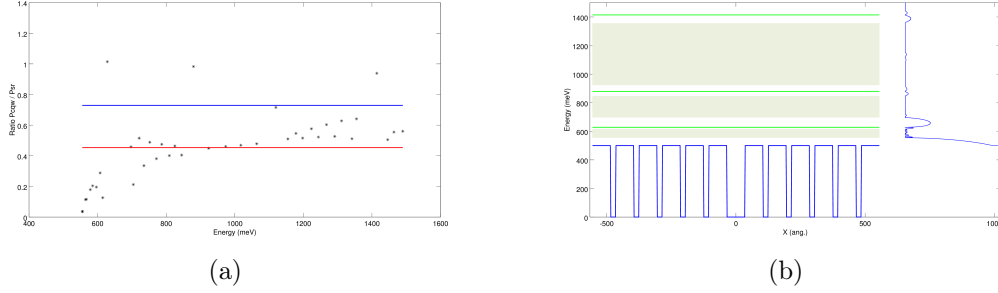
Figure 4.6: Simulation result of superlattice example. The aproximate method result in (a) and (b) the final energy-band configuration.

Table 4.2 exhibits the energy values of the discrete energy levels and minibands detected by the algorithm.

Energy Value	Localizated State
555.25	Beginning of Miniband
615.07	End of Miniband
628.22	Discrete Energy Level
697.35	Beginning of Miniband
845.08	End of Miniband
879.46	Discrete Energy Level
924.12	Beginning of Miniband
1354.92	End of Miniband
1414.28	Discrete Energy Level

Table 4.2: Fitness calculation example.

To set the λ value, it was used a dataset with 200 examples, provided by professor Marcelo Maialle. Each example is a superlattice of quantum wells with different geometry. For each structure, λ was tight to achieve the correct identification of the energy-band configuration. Then, the mean of the set of λ obtained, when all examples were correctly detected, was computed. This value was used to set the final λ value, 1.2.

4.2   Optimization Model

To accomplish the correct function of the GA, two fundamental details are important:
the chromosome and the fitness function.

The chromosome of an individual is the abstraction of the parameters to be
optimized in the real world problem. Thus, the chromosome to achieve the SPQW
optimization is composed by 5 genes as illustrated in the Figure 4.7 and detailed in
Table 4.3. For the structures studied in this work the numbers of quantum wells is a
symmetrical parameter, i.e, the number of the quantum wells to the right of the central
quantum well are the same in the left. For example, 5 quantum wells indicate that the
structure will be composed by the central quantum well and 5 quantum wells to the
right and to left of it, as detailed in the example of the Section 4.1.2.

Gene 1	Gene 2	Gene 3	Gene 4	Gene 5
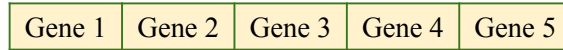
Figure 4.7: Chromosome representation.

Table 4.3 explains the boundary conditions of the individual parameters, these
ranges were defined in talks with professor Marcelo Maialle.

Gene	Description	Ranges
g1	Number of Quantum Wells	[5 , 15]
g2	Central Quantum Well Width (Ang.)	[10 , 40]
g3	Barriers Width (Ang.)	[20 , 90]
g4	Barriers Height (meV)	[400 , 600]
g5	Superlattice of Quantum Wells Width (Ang.)	[20 , 70]

Table 4.3: Individual parameters and their boundary conditions.

In order to simplify the optimization process all variables are limited to real num-
bers ranging from 0 to 1 which are latter interpolated to match superlattice attributes.

To evaluate each individual the method described in Section 4.1.2 is used and the
following fitness function is computed:

$$Fitness(E_{(g1,g2,g3,g4,g5)}, X_{(g1,g2,g3,g4,g5)}) = \sum (1 - x_i) \cdot (e_i - e_{i-1}) + x \cdot \theta(e_i - e_{i-1}) \quad (4.4)$$

where E is the set with the energy values obtained for the specific structure configu-
ration, X a is a set indicating if the energy value is a discrete state, e_i is the energy

value of the *ith* beginning of miniband detected, $x_i = 0$ if the energy value e_{i-1} is a discrete level, or $x_i = 1$ if e_{i-1} is the end of a miniband, θ is an empirical parameter to penalize the error when not desired structures are found.

Thus, the fitness calculation for the same structure example explained in the Section 4.1.2 and for $\theta = 1.5$, is detailed above:

$$Fitness(E_{(5,70,70,500,20)}, X_{(5,70,70,500,20)}) = ((555.25-500)\cdot 1.5)+(697.35-628.22)+(924.12-879.46) = 140.70 \quad (4.5)$$

For the cases in that the first energy level is the beginning of a miniband, as evidenced in this example, the height of the barriers is used as reference to calculate the gap between them.

Then, the optimization target of the GA is to minimize the *Fitness* function, formally:

$$Solution = min(Fitness(E_{(g1,g2,g3,g4,g5)}, X_{(g1,g2,g3,g4,g5)})) \quad (4.6)$$

Once defined, the genetic algorithm, initially, creates a set of randomly generated individuals to compose the initial population. Individuals are then evaluated and selected based in their fitness to create couples and have their genes crossed to generate new individuals. Thus, each couple selected perform the crossover procedure where each gene for each son is computed according to:

$$Son_1 = R \cdot Parent1 + (1-R) \cdot Parent2 \quad (4.7)$$

$$Son_2 = (1-R) \cdot Parent1 + R \cdot Parent2 \quad (4.8)$$

where R is a random value between 0 and 1.

This crossover is always performed when new individuals are needed to create a new population. In order to broaden the search, these new individuals generated are randomly chosen to perform mutation. In the mutation process, genes are chosen to receive a new value. It has been applied, in this work, three kinds of mutation: uniform mutation, non-uniform mutation and side-shift mutation.

Non-uniform mutation, as described in Michalewicz [2013], is a technique to make a fine search and ensure that at least a local optimum is reached. So a gene v is selected through a mutation rate, and then applying the following equation to compute the new

value.

$$v' = \begin{cases} v + \delta(t, UB - v), & \text{if random value } 0 \\ v - \delta(t, v - LB), & \text{if random value } 1 \end{cases} \tag{4.9}$$

where LB and UB are lower and upper domain bounds for variable v. t represents the generation number. The function $\delta(t, y)$, described in equation 4.10 returns a value in the range $[0, y]$ that rapidly approaches 0 as the end of generations draws near. In this way, we allow our search to spread in the space initially and very locally at later stages; thus tunning the search to minor steps, which brings benefits when minimum and maximum can be very near on the search space.

$$\delta(t, y) = y \cdot (1 - r^{(1 - \frac{t}{\tau})^b}) \tag{4.10}$$

In this equation, t is the current generation, y is the maximum value that the function can return, r is a random number from $[0..1]$, τ is the maximal generation number, and b is a system parameter determining the strengh of the shift that is going to happen in the gene.

Finally, elitism is ensured by always copying a number of best individuals from the last generation to the current generation.

4.3   Simulation Results

To find superlattices of quantum wells structures with specific energy-band configuration, the genetic algorithm described in Section 4.2 has been applied in conjunction with the simulation method explained in Section 4.1.2.

The parameters used to set up the GA, for all experiments, are detailed in Table 4.4.

Number of individuals per generation	50
Number of generations	150
Elitist set length	5
Mutation rate	15%
Uniform mutation rate	50%
Non-uniform mutation rate	50%

Table 4.4: Genetic algorithm parameters

The elistist set length represents the size of the set of the best individuals in the current population which can never be selected to be replaced. This procedure ensures

an elitist behavior, thus, preserving the evolution of the population.

The mutation rates described above means that 15% of the newly generated individuals are chosen to be mutated and among those, 50% are going to be uniformly mutated and the other 50% will be non-uniformly mutated.

By applying these parameters in the genetic algorithm, during the course of three months it was possible to run eight experiments whose details are displayed in Table 4.5. For each experiment is detailed, the duration in days, the number of individuals evaluated and the the best fitness found. These experiment were performed in a machine with Ubuntu 12.04, 16 GB of memory RAM and processor Intel Core i7-2600 CPU @ 3.40GHz. A superlattice of quantum wells simulation is carried-out in about 3 minutes.

Experiment	Duration (days)	Evaluation's amount	Best individual found
1	15	7524	92.9807
2	12	6983	97.6952
3	14	7247	219.3430
4	15	7431	152.6827
5	14	7302	120.7379
6	13	6925	85.7514
7	13	6896	84.6815
8	13	6915	143.3456

Table 4.5: Experiment results.

For these experiments two different values of the penalization in the fitness function were used. In this way, for the experiments 1,2,3 and 4 θ was set in 0.6 and for the other experiments was set in 1.5. An important note is that when the θ value was set in 0.6, structures with not desired energy-band configurations were found.

Figures 4.8a and 4.8b are results of the fitness curves, for the θ values of 0.6 and 1.5, respectively. In these curves, it is shown how each strategy evolved in an average of the best individuals from each generation.

The parameters of the best structure found in these experiments are shown in Table 4.6. In Table 4.7, the energy levels detected and the fitness value of this structure are detailed. Figure 4.9 illustrated the energy-band localization and the transmission coefficient for this structure.

In contrast, the worst structure found in the optimization process was detailed in Table 4.8 and in Table 4.9. Also, Figure 4.10 shows the energy-band localization and the transmission coefficient for this structure.
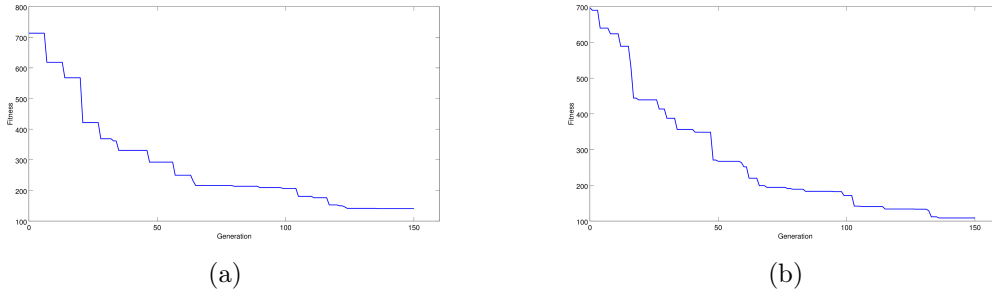
Figure 4.8: Genetic algorithm evolution (a) with penalization 0.6. and (b) 1.5.

Number of Quantum Wells	7
Central Quantum Well Width	63 Ang.
Superlattices of Quantum Wells Width	16 Ang.
Barriers Width	48 Ang.
Barriers Height	501 meV

Table 4.6: Parameters of the best individual found.

	Energy Value	Localizated State
	547.12	Discrete Energy Level
	612.23	Beginning of Miniband
	774.97	End of Miniband
	862.08	Discrete Energy Level
	881.65	Beginning of Miniband
	1163.71	End of Miniband
Fitness Value	84.6815	

Table 4.7: Simulation result of the best individual found.

Number of Quantum Wells	8
Central Quantum Well Width	62 Ang.
Superlattices of Quantum Wells Width	16 Ang.
Barriers Width	51 Ang.
Barriers Height	495 meV

Table 4.8: Parameters of the worst individual found.

These results demonstrate that an genetic algorithm is an adequate technique to optimization of superlattices with central quantum well. The best structures found here have great potential to be grown experimentally and to develop optoelectronic devices such as photodetectors. The evolution curves of the GA shows that the minimization target is accomplished. It was detected that the penalization in the fitness function
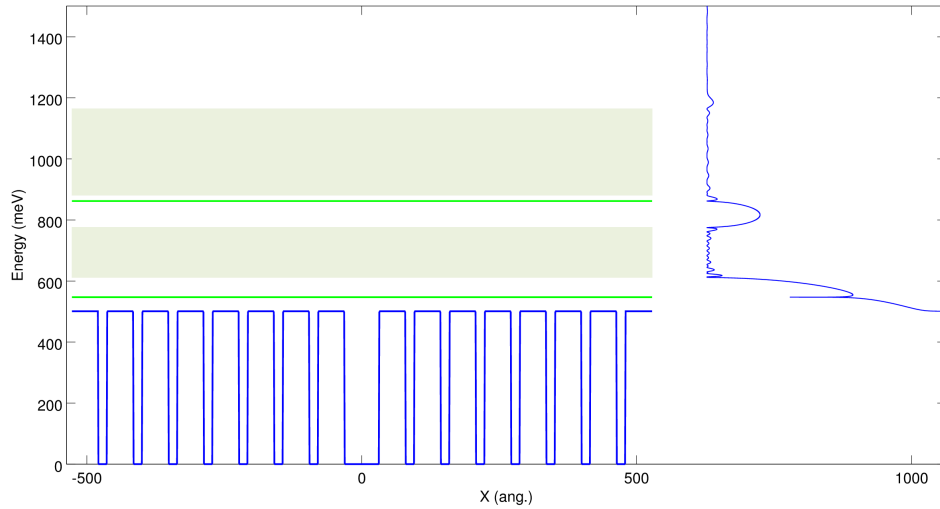
Figure 4.9: Energy-band localization of the best individual.

Energy Value	Localizated State
546.08	Discrete Energy Level
596.99	Beginning of Miniband
749.32	End of Miniband
835.74	Beginning of Miniband Discrete
1090.00	End of Miniband
1120.40	Discrete Energy Level
1170.32	Beginning of Miniband Discrete
1451.00	End of Miniband

	Fitness Value	152.6827

Table 4.9: Simulation result of the worst individual found.

is a critical parameter for the performance of the GA. This parameter was set in 0.6, initially, under the premise to produce generations with great diversification and to scape from a local minima. For the experiments in that θ was set with this value, in two of theirs interesting results with the desired characteristics were obtained, but in the other two cases individuals with not desired energy-band configurations were kept along the evolution process and returned as the best solution. When θ was set in 1.5, structures with the desired characteristics were found. Due to the high computational cost to perform an optimization experiment, bigger θ values were not evaluated. In the superlattices with central quantum well studied in this work, only the energy levels above the miniband are considered.
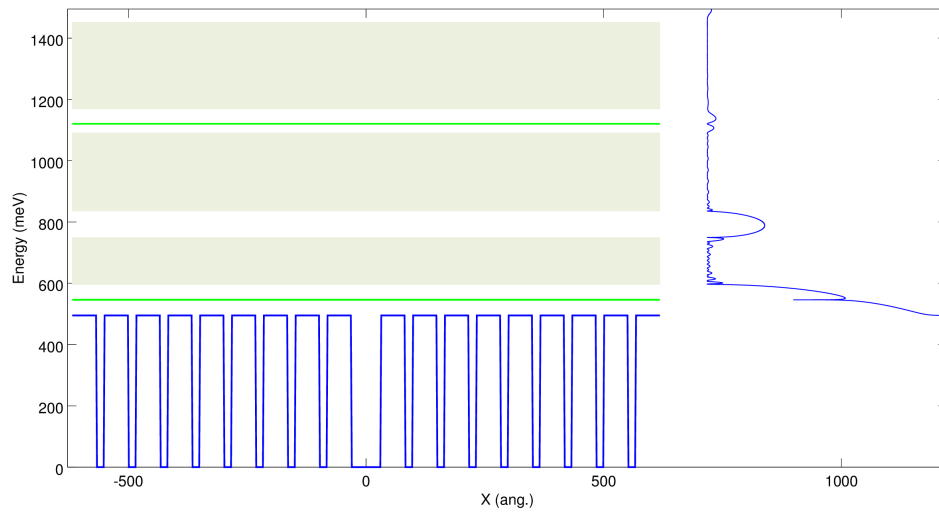
Figure 4.10: Energy-band localization of the worst individual.

Chapter 5

Logic Devices with Photonic Crystals

This chapter presents the process to accomplish the all-optical logic gates in photonic crystals, the results of the Majority and Feynman gates proposed in this work and a methodology to be applied for the robustness analysis of all-optical logic devices in photonic crystals.

5.1   Majority and Feynman Gates

The realization of the logic gates can be achieved due to the photonic crystal waveguide, which takes advantage of the controlled light beam interference effect. For the development of all-optical Majority and Feyman gates, we use a two-dimensional photonic crystal.

According to wave optics theory, if the phase difference between two light beams is $2k\pi$ (where $k = 0, 1, 2, ...$), then constructive interference will occur, and the output light will have high power (corresponding to the logic state of 1). If the phase difference is $(2k + 1)\pi$ (where $k = 0, 1, 2, ...$), then destructive interference will occur, and the output light will be approximately zero (corresponding to the logic state of 0) Zeng et al. [2010].

Photonic crystal structures studied here are composed of triangular lattice arrays of cylindrical silicon rods embedded in a background medium of air. The lattice constant a is 875 nm and the diameter of the silicon rods are 495 nm. The dielectric constant of silicon and air are set as 11.56 and 1, respectively. The wavelength, λ, supported by the waveguide of this structure, corresponding to the photonic band

gap, is 1550 nm, as used in the optical communications window. These are the same parameters used by Fu et al. [2013].

For the study of the electric field distribution of the photonic crystal structure, the simulations were carried out with the finite difference time-domain (FDTD) method using the MIT software package, MEEP, described by Oskooi et al. [2010]. MEEP can solve numerically Maxwell's equations, used to calculate transmission and reflection spectra, resonant modes and frequencies, and field patterns (e.g. Green's functions) in response to an arbitrary source, typically a continuous (CW) or Gaussian wave input. Also, MEEP will discretize this structure in space and time, and that is specified by a single variable, the resolution. The resolution used here was set as 40.

To set a logic input in 1 a CW, with frequency $\frac{ac}{\lambda}$ ($c = 1$) for units in MEEP, is applied. Finally, to get the transmission output, the flux spectra is computed in the output point of the structure with the design of the logic device (F_d) and without it (F_{wd}), then the ratio F_d/F_{wd} is calculated.

5.1.1   Majority Gate

The Majority gate is a logic device with three inputs and one output. The output is the majority function, thus, if at least two inputs are 0 then the output is 0. In contrast, the output is 1 if and only if at least two inputs are 1. Table 5.1 present the truth table for this logic function.

A	B	C	Y
0	0	0	**0**
0	0	1	**0**
0	1	0	**0**
0	1	1	**1**
1	0	0	**0**
1	0	1	**1**
1	1	0	**1**
1	1	1	**1**

Table 5.1: Majority gate truth table.

Observe that, if one input is fixed at binary 0 an AND gate with two inputs is defined. In the same way, if one input is fixed at binary 1, an OR gate is accomplished. This property allows the creation of simple and optimized computational circuits. Majority gate is a basic logic device in other technologies, such as Quantum dot Cellular Automata (QCA). In the same way, we believe that majority gates can be used to design optimized computational circuits in photonic crystals.

The schematic structure for the all-optical Majority gate is shown in Figure 5.1a. It is formed by three symmetrical optical waveguides: AY, BY, CY, of equal length.

(a)   (b)

(c)   (d)

(e)   (f)

(g)   (h)
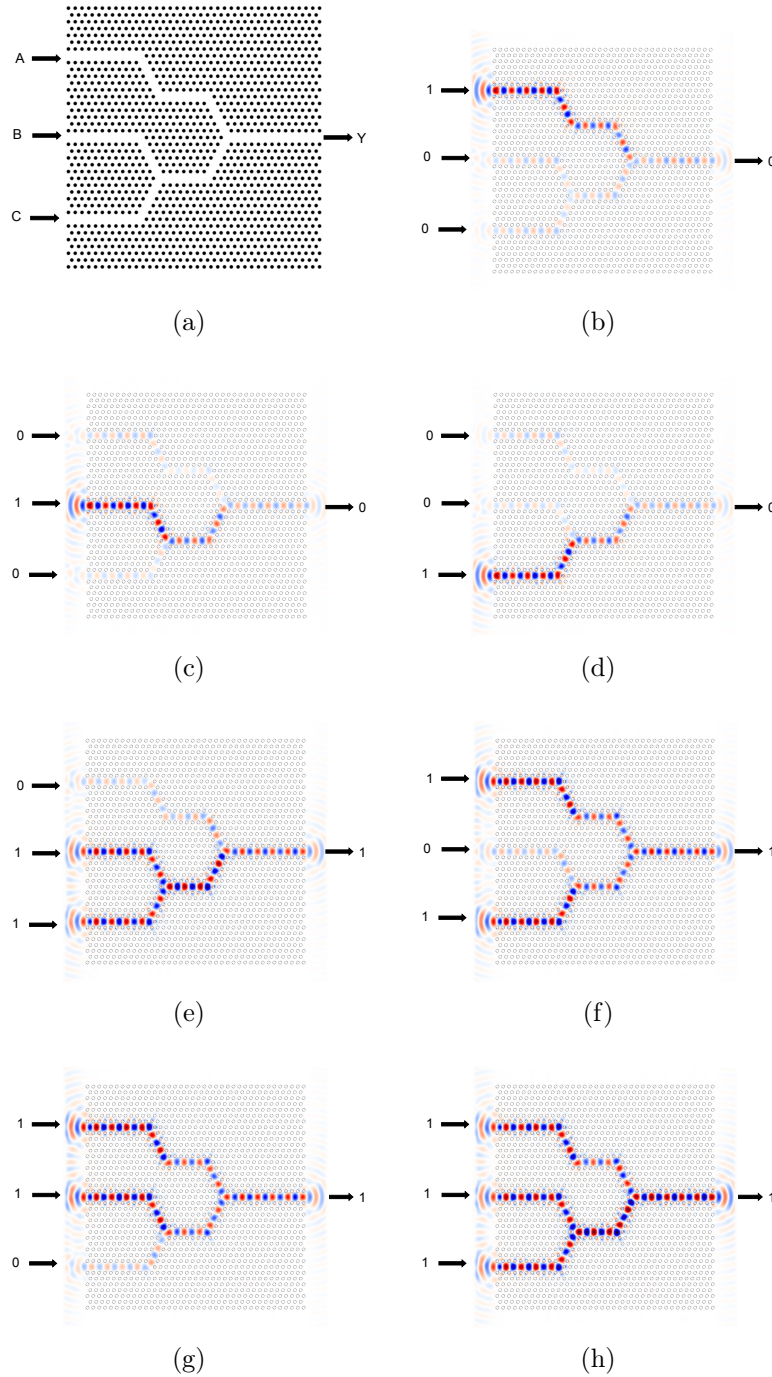
Figure 5.1: Majority gate simulation results.

Considering the input set $(1, 0, 0)$, a single beam is injected into input port A, then the signal light can propagate through the optical waveguide AY to the output

Y. There are losses in the way, reaching output Y with transmission smaller than 0.35. These correspond to a logic operation $Maj(1,0,0) = 0$, as shown in Figure 5.1b.

Similarly, if a single beam is injected into input port B or C, the signal light can propagate through the optical waveguide BY and CY, respectively, to the output Y with low transmission. These correspond to logic operations $Maj(0,1,0) = 0$ and $Maj(0,0,1) = 0$, as shown in Figure 5.1c and Figure 5.1d.

When two beams are injected into two inputs ports, then the phase difference of these two signal light beams is zero. Constructive interference occurs, and the output signal has a transmission greater than 0.85, as shown in Figure 5.1e, Figure 5.1f and Figure 5.1g. This corresponds to the logic operations $Maj(0,1,1) = 1$, $Maj(1,0,1) = 1$, $Maj(1,1,0) = 1$.

Finally, if the beams are injected into the three inputs ports, then the phase difference at the cross point is zero, causing a constructive interference, and achieving 1.00 of transmission. This corresponds to $Maj(1,1,1) = 1$, shown in Figure 5.1h. Obviously, when no single beam is injected in any input port, then no light comes to output, corresponding to $Maj(0,0,0) = 0$.

Table 5.2 summarizes the transmission results for the Majority gate. When the transmission output is greater than 0.85 it is considered as logic output 1. If the transmission output is less than 0.35, then it is considered as logic output 0.

Input (A,B,C)	Output Y	Transmission
(0,0,0)	0	0
(0,0,1)	0	0.32
(0,1,0)	0	0.32
(0,1,1)	1	0.88
(1,0,0)	0	0.32
(1,1,0)	1	0.95
(1,0,1)	1	0.95
(1,1,1)	1	1.00

Table 5.2: Transmission results for all-optical majority gate

5.1.2   Feynman Gate

In 1961, Rolf Landauer argued that any irreversible computational process, e.g., AND, OR, XOR, implies the loss of $K_B T Ln2$ joules per bit erased, where K_B is the Boltzmann constant and T is the temperature, see Neumann [1966]. One possible solution is achieved by building the process using reversible primitives. These primitives, also

known as reversible gates, are information preserving, i.e., they have one-to-one relation (bijective functions) between inputs and outputs.

The Feynman gate is a logic reversible device with two inputs (A,B) and two outputs (X,Y). The outputs are defined by the function $X = A$ and $Y = A \oplus B$. Table 5.3 illustrate the truth table for the Feynman logic gate.

A	B	X	Y
0	0	**0**	**0**
0	1	**0**	**1**
1	0	**1**	**1**
1	1	**1**	**0**

Table 5.3: Feynman gate truth table.

Photonic crystals have been seen as a promising technology for approaching the thermodynamic limit of computation, thus in an effort to go beyond that limit we propose an all-optical Feynman gate, shown in Figure 5.2a. To the best of our knowledge, it is the first time that a reversible gate is proposed based on photonic crystals.

(a)

(b)

(c)

(d)
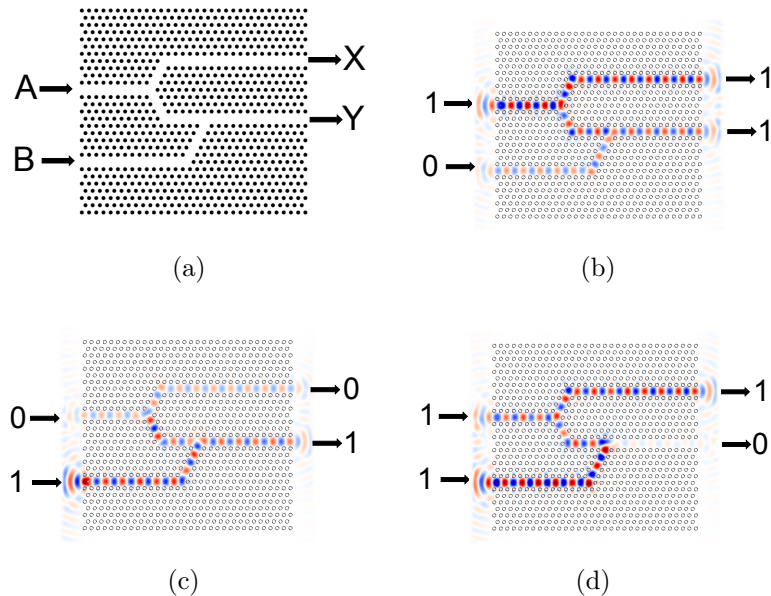
Figure 5.2: Feynman gate simulation results.

When a single beam is injected into input port A, then the optical signal propagates to both outputs X and Y with transmission greater than 0.40, as shown in Figure 5.2b. This corresponds to the logic operation $Feyn(1,0) = (1,1)$. If a single light beam is injected into input port B, then the optical signal propagates to the output X

and Y, with transmission of 0.10 and 0.50, respectively. This corresponds to the logic operation $Feyn(0,1) = (0,1)$, as shown in Figure 5.2c.

When the two input ports are excited, then the difference of the path length between the waveguide AY and BY is one lattice constant, and the phase difference is π. Thus, destructive interference occurs and the transmission in the output Y is only 0.01. The transmission at the output X is 0.75. This corresponds to the logic operation $Feyn(1,1) = (1,0)$, as shown in Figure 5.2d. Finally, if no single beam is injected in both input ports, then no light comes to the output, corresponding to $Feyn(0,0) = (0,0)$.

Table 5.4 presents the results for the transmission of the all-optical Feynman gate. It is possible to observe that transmissions $\geq 40\%$ are considered as logic output 1, and $\leq 10\%$ are considered as logic 0.

Input (A,B)	Output (X,Y)	Transmission X	Transmission Y
(0,0)	(0,0)	0	0
(0,1)	(0,1)	0.10	0.50
(1,0)	(1,1)	0.45	0.40
(1,1)	(1,0)	0.75	0.01

Table 5.4: Transmission results for all-optical Feynman gate

5.2   Robustness Analysis of All-Optical Logic Gates

The process of robustness analysis proposed here is a methodology to identify critical regions and evaluate the reliability and fault tolerance of the all-optical logic devices designed with photonic crystals waveguides. This is a relevant step before the physical growth of these devices, because allows to know and measure the behaviour of them due to possible errors or disorders added in the system.

Generally, the logic gates projected in two-dimensional photonic crystals are composed of triangular or square lattice arrays of cylindrical semiconductor rods embedded in a background medium of air. On the other hand, they also can be projected with triangular or square lattice arrays of cylindrical air holes embedded in a background medium of a semiconductor material. The disorders consist in horizontal and vertical displacements, reduction and enlargement of the cylinders that form the device.

Then, to cause disorders in the system, random numbers are generated with the following Gaussian distribution:

$$\delta = ae^{\frac{(x-b)^2}{2c^2}} \tag{5.1}$$

where $a = \frac{1}{\sigma\sqrt{2\pi}}$, $b = \mu$, $c = \sigma$ and x the input, μ and σ are the center and the width of the function, respectively, as can be observed in the Figure 5.3.
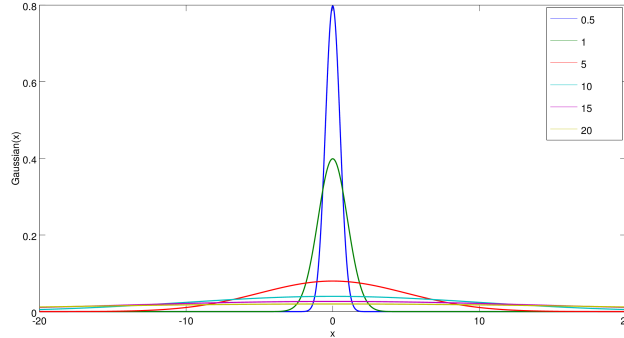
Figure 5.3: Gaussian distribution for $\sigma = (0.5, 1.0, 5.0, 10.0, 15.0, 20.0)$.

This distribution allows to control the μ and σ parameters. In this work, μ is setted as 0 and σ a set of variable parameters: $(0.5, 1.0, 10.0, 15.0, 20.0)$. It is important to note that bigger σ values can cause uncontrollable behaviours in the system. Thus, the formal expression that describes the disorder added to a cylinder for each component is:

$$f(x, y, r) = (x \pm \delta x(0, \sigma))_x + (y \pm \delta y(0, \sigma))_y + (r \pm \delta r(0, \sigma))_r \qquad (5.2)$$

where x and y are the cartesian coordinates of the cylinder position and r the radius. It is important to remark that $\delta(0, 20)$ generates disorders about ± 80 nm.

When these disorders appear in the growth and/or fabrication process, the correct operation of the device probably will be affected. That is, the output transmission expected values can change significantly. To consider an error in the output transmission a tolerance value is defined, setted in 0.1, as in electronic devices. So, for each study case of each logic gate, 50 simulations are performed, as indicated by Jain [1991], and a statistical test is computed to measure the reliability and robustness of the device. The statistical test consist in calculate the mean, standard deviation and confidence interval with 95% of confidence level for each study case. Then, the tolerance value is evaluated with respect to the expected value.

For example, if the transmission output of a device without disorders is 0.8, interpreted as logic 1, but the obtained expected value includes includes smaller values that the tolerance, (0.7 for this case), it can be said with 95% of confidence level that the logic device probably operates unexpectedly, as illustrated in Figure 5.4a. On the other hand, if the transmission output of a device without disorders is 0.8, interpreted

as logic 0, but the obtained expected value includes includes smaller values that the tolerance, (0.7 for this case), it can be said with 95% of confidence level that the logic device probably operates unexpectedly, as shown in Figure 5.4b.

(a)   (b)
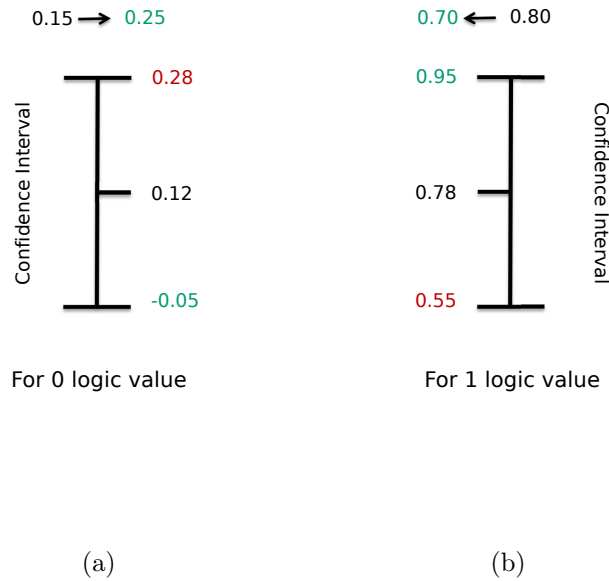
Figure 5.4: Robustness Analysis test. (a) for output transmission interpreted as logic 1 and (b) logic 0.

5.2.1   OR Gate

To accomplish the robustness analysis of the OR logic device proposed by Fu et al. [2013], the first three study cases are illustrated in Figure 5.5.

It is important to remember that the OR is a symmetrical logic device, i.e., the transmission and the path difference are equal for the inputs, $(0, 1)$ and $(1, 0)$. The output transmission for $(0, 1) - (1, 0)$ input cases is: 0.411 and for input $(1, 1)$ is 0.846. Then, output transmission greater than 0.4 and is considered as logic 1. The lower boundary of the tolerance to consider an error is 0.3.

The mean, standard deviation and the confidence interval, computed with 95% of confidence level, are described in Table 5.5 for the $(0, 1)$ and $(1, 1)$ input cases, lines 1,2,3 and for all cylinders. The numbers in red represent the cases when the tolerance value is infringed, in yellow when they are close to the limits, while when the expected value is close to the real transmission it is shown in green.
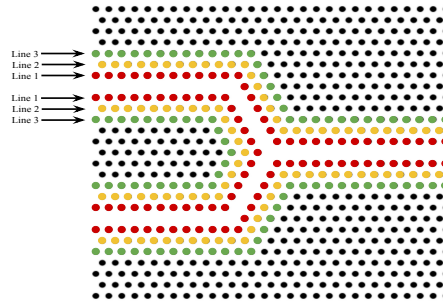
Figure 5.5: Lines analysed for the OR device.

		(0,1)						(1,1)					
		σ						σ					
Region		0.50	1.00	5.00	10.0	15.0	20.0	0.50	1.00	5.00	10.0	15.0	20.0
All	Mean	0.411	0.411	0.411	0.408	0.385	0.335	0.846	0.846	0.845	0.833	0.773	0.450
	Std	0.002	0.004	0.019	0.044	0.076	0.181	0.002	0.003	0.016	0.037	0.095	0.276
	CI	**0.408**	**0.402**	0.375	0.322	0.237	**-0.019**	**0.841**	**0.840**	0.814	0.760	0.587	**-0.091**
		0.415	**0.420**	0.447	0.495	0.534	**0.689**	**0.850**	**0.852**	0.876	0.905	0.959	**0.990**
Line 1	Mean	0.409	0.409	0.408	0.402	0.382	0.313	0.841	0.841	0.836	0.808	0.763	0.530
	Std	0.002	0.004	0.020	0.033	0.094	0.187	0.002	0.003	0.017	0.041	0.107	0.237
	CI	**0.405**	**0.401**	0.368	0.337	0.198	**-0.053**	**0.838**	**0.834**	0.802	0.729	0.553	**0.065**
		0.413	**0.417**	0.448	0.467	0.566	**0.679**	**0.845**	**0.847**	0.870	0.888	0.974	**0.995**
Line 2	Mean	0.411	0.411	0.411	0.412	0.411	0.399	0.846	0.846	0.846	0.846	0.852	0.820
	Std	0.000	0.000	0.002	0.004	0.007	0.071	0.000	0.001	0.002	0.005	0.026	0.091
	CI	**0.411**	**0.410**	**0.407**	**0.404**	0.397	0.259	**0.845**	**0.845**	**0.842**	**0.837**	0.801	0.641
		0.412	**0.412**	**0.415**	**0.419**	0.426	0.539	**0.846**	**0.847**	**0.850**	**0.856**	0.903	0.999
Line 3	Mean	0.411	0.411	0.411	0.411	0.411	0.409	0.846	0.846	0.846	0.846	0.846	0.842
	Std	0.000	0.000	0.000	0.000	0.001	0.006	0.000	0.000	0.000	0.000	0.001	0.008
	CI	**0.411**	**0.411**	**0.411**	**0.411**	**0.409**	0.397	**0.846**	**0.846**	**0.846**	**0.846**	**0.844**	0.826
		0.411	**0.411**	**0.411**	**0.411**	**0.412**	0.421	**0.846**	**0.846**	**0.846**	**0.846**	**0.847**	0.858

Table 5.5: Simulations results for the modifications of the all cylinder and the first three lines for the OR device. Std is the standard deviation and CI the confidence interval.

For the input $(0, 1)$ when all cylinders are modified with $\sigma = [15, 20]$ the expected transmission value includes 0.3. Then the lower boundary of tolerance is infringed as a result of a high standard deviation, due to low transmission values obtained. Thus, with 95% of confidence level, it can be said that the system probably operates unexpectedly. When the disorders are added using $(0.5 \leq \sigma \leq 10)$ the performance of the device is not affected, at the same confidence level.

If the disorders are added in the first line the same considerations are valid.

For the second line, only disorders with $\sigma = 20$ can produce output transmission

that infringe the lower tolerance value. Modifications in the second line with $(0.5 \leq \sigma \leq 15)$ are not significant.

Finally, it can be said with 95% of confidence level that the cylinders of the third line do not affect the correct operation of the device applying disorders in the interval $(0.5 \leq \sigma \leq 20)$.

For the input $(1, 1)$, two cases must be evaluated. The first, when the general lower limit of the tolerance is infringed, i.e. 0.3, and the second when the transmission is under 0.75, that is, the lower boundary of tolerance for the input $(1, 1)$. Then, when all cylinders are modified with $\sigma = 20$ the two lower boundary conditions are infringed as a result of a high standard deviation, due to low transmission values obtained and the confidence interval includes 0.3 and 0.75. Thus, with 95% of confidence level, it can be said that the system probably operates unexpectedly. When the modifications are in the order of $\sigma = 15$ the lower limit of tolerance for this input case is infringed, but note that the low transmission value can be interpreted as logic 1. The results show that applying disorders in the interval $(0.5 \leq \sigma \leq 10)$ the device operates as projected.

When the cylinders of the first line are modified using $\sigma = 20$ the two lower boundary conditions are infringed. On the other hand, if modifications with $\sigma = [10, 15]$ are applied the lower boundary condition for the input case in infringed but the low transmission expected can be interpreted as logic 1. When the disorders are applied in the interval $(0.5 \leq \sigma \leq 5)$ the correct operation of the device is accomplished.

For the second line, only disorders with $\sigma = 20$ can produce output transmission that infringe the lower tolerance value for the input case. Modifications in the second line with $(0.5 \leq \sigma \leq 15)$ can be despicable.

The disorders application in the third line can be ignored with 95% of confidence level.

As previously demonstrated, the cylinders of the first line have greater effect in the performance of the device by the reason that they are closer to the waveguide. Then, five regions are analysed to establish which of them have the greatest effect in the device performance, illustrated in Figure 5.6.
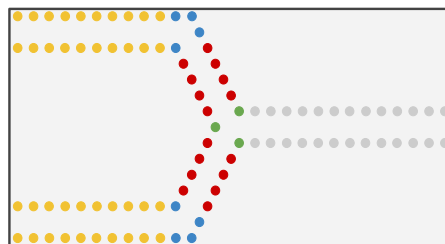
Figure 5.6: Regions analysed for the OR device.

The first, in yellow, is formed by the first ten cylinders of the waveguide input. The second, in red, by the four cylinders that form the inclination of the waveguide input. The third, in gray, by the thirteen cylinders of the output. The fourth, in blue, is composed by the four cylinders that form the edge of the waveguide. The fifth is formed by the four cylinders of the inputs intersection, in green. As can been observed in the simulations results shown above, modifications with $\sigma = 20$ generates greater effects. Due to the high computational cost to perform these experiments, only modifications of this order are investigated. The results for these regions are displayed in Table 5.6.

		(0,1)	(1,1)
		σ	σ
Region		**20.0**	**20.00**
1	Mean	0.332	0.604
1	Std	0.065	0.121
1	CI	**0.205**	**0.369**
1		**0.461**	**0.841**
2	Mean	0.348	0.668
2	Std	0.065	0.055
2	CI	**0.220**	**0.560**
2		**0.476**	**0.776**
3	Mean	0.313	0.609
3	Std	0.041	0.134
3	CI	**0.233**	**0.346**
3		**0.394**	**0.872**
4	Mean	0.322	0.657
4	Std	0.062	0.045
4	CI	**0.201**	**0.569**
4		**0.444**	**0.745**
5	Mean	0.310	0.653
5	Std	0.073	0.081
5	CI	**0.169**	**0.495**
5		**0.453**	**0.811**

Table 5.6: Simulations results of the first line regions for the OR device. Std is the standard deviation and CI the confidence interval.

For these regions it is important to note that in average the transmission results are close to the value when the first line is analysed completely. The regions with greater impact for the input case $(0, 1)$, as shown in Figure 5.7b, are the 3 and 5. For the $(1, 1)$ input case the regions with greater effect are the 1 and 3, as illustrated in Figure 5.7c.

Figure 5.7a shows the normalized average of the OR logic gate, as can observed, the third region have greater effect for both input cases by the reason that the device is projected with triangular lattice and the periodicity in the straight lines can be easily broken.

(a)

(b)

(c)
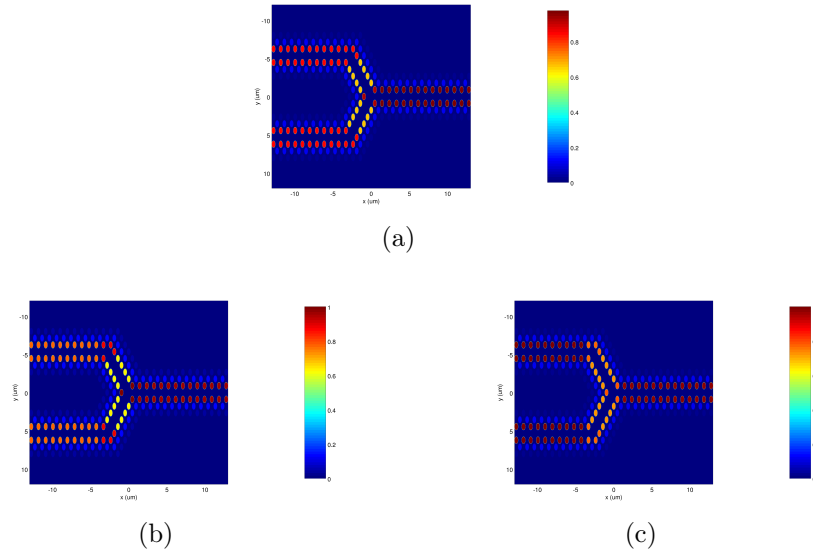
Figure 5.7: Regions effect for the OR device. (a) Normalized average. (b) Input case (0,1). (c) Input case (1,1).

5.2.2   XOR Gate

For the XOR logic device proposed by Fu et al. [2013], the lines to be analysed are detailed in Figure 5.8. It is important to remember that the output transmission for the XOR logic device are: 0.318 for the (0,1) input case, 0.858 for the (1,0) input case and 0.067 for the (1,1) input case. Then output transmission greater than 0.3 and lower than 0.07 are interpreted as logic 1 and 0, respectively. The lower boundary of the tolerance to consider an error is 0.2 for the cases when the logical output is 1 and the upper limit of tolerance 0.17 for the cases when the logical output is 0.

The mean, standard deviation and the confidence interval, computed with 95% of confidence level, are described in Table 5.7 for the $(0,1)$ and $(1,0)$ input cases, lines 1,2,3 and for all cylinders.

For the input $(0,1)$ when all cylinders are modified with $\sigma = [10, 15, 20]$ the lower boundary of tolerance is infringed as a result of a high standard deviation, due to low transmission values obtained and the confidence interval includes 0.2. Thus, with 95% of confidence level, it can be said that the system probably operates unexpectedly. In contrast, when the disorders are added using $(0.5 \leq \sigma \leq 5)$ the performance of the
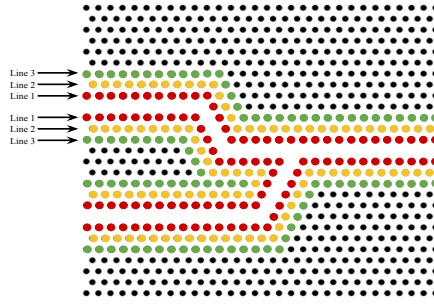
Figure 5.8: Lines analysed for the XOR device.

		(0,1)						(1,0)					
		σ						σ					
Region		**0.50**	**1.00**	**5.00**	**10.0**	**15.0**	**20.0**	**0.50**	**1.00**	**5.00**	**10.0**	**15.0**	**20.0**
All	**Mean**	0.317	0.317	0.311	0.306	0.310	0.304	0.857	0.856	0.853	0.837	0.775	0.508
	Std	0.003	0.007	0.035	0.068	0.109	0.245	0.002	0.005	0.024	0.049	0.120	0.304
	CI	**0.310**	**0.303**	0.242	0.171	0.096	**-0.176**	**0.852**	**0.845**	0.804	0.739	0.539	**-0.088**
		0.324	**0.331**	0.380	0.441	0.524	**0.785**	**0.862**	**0.867**	0.901	0.934	1.012	**1.104**
Line 1	**Mean**	0.318	0.315	0.318	0.310	0.313	0.309	0.857	0.855	0.847	0.831	0.721	0.465
	Std	0.003	0.006	0.038	0.071	0.109	0.249	0.002	0.004	0.022	0.045	0.144	0.302
	CI	**0.312**	**0.303**	0.242	0.169	0.099	**-0.179**	**0.852**	**0.847**	0.802	0.741	0.437	**-0.128**
		0.324	**0.328**	0.393	0.450	0.527	**0.798**	**0.862**	**0.864**	0.891	0.920	1.005	**1.059**
Line 2	**Mean**	0.317	0.318	0.317	0.316	0.316	0.307	0.857	0.857	0.856	0.857	0.851	0.833
	Std	0.000	0.000	0.002	0.005	0.009	0.070	0.000	0.000	0.002	0.004	0.074	0.123
	CI	**0.317**	**0.317**	**0.313**	0.305	0.298	0.169	**0.857**	**0.856**	**0.851**	0.848	0.705	0.591
		0.318	**0.318**	**0.321**	0.326	0.335	0.444	**0.858**	**0.858**	**0.861**	0.867	0.998	1.074
Line 3	**Mean**	0.317	0.317	0.317	0.317	0.317	0.315	0.857	0.857	0.857	0.857	0.857	0.856
	Std	0.000	0.000	0.000	0.000	0.002	0.003	0.000	0.000	0.000	0.000	0.001	0.012
	CI	**0.317**	**0.317**	**0.317**	**0.317**	0.311	0.308	**0.857**	**0.857**	**0.857**	**0.857**	0.855	0.831
		0.317	**0.317**	**0.317**	**0.317**	0.318	0.323	**0.857**	**0.857**	**0.857**	**0.857**	0.858	0.881

Table 5.7: Simulation results for the modifications of all cylinders and the first three lines for the XOR device and (0,1) and (1,0) input cases. Std is the standard deviation and CI the confidence interval.

device is not affected. If the disorders are added in the first line, the same considerations are valid.

For the second line, only disorders with $\sigma = 20$ can produce output transmission that infringe the lower tolerance value. Modifications in the second line with ($0.5 \leq \sigma \leq 15$) can be neglected.

Finally, it can be said with 95% of confidence level that the cylinders of the third line do not affect the correct operation of the device, applying disorders in the interval ($0.5 \leq \sigma \leq 20$).

For the input $(1, 0)$, two cases must be evaluated. The first, when the general lower limit of the tolerance is infringed, i.e. 0.3, and the second when the transmission is under 0.75, that is, the lower boundary of tolerance for the input $(1, 0)$. Then, when all cylinders are modified with $\sigma = 20$ the two lower boundary conditions are infringed as a result of a high standard deviation, due to low transmission values obtained and the confidence interval includes 0.2. Thus, with 95% of confidence level, it can be said that the system probably operates unexpectedly. When the modifications are in the order of $\sigma = [10, 15]$ the lower limit of tolerance for this input case is infringed, nevertheless the low transmission value can be interpreted as logic 1. The results show that applying disorders in the interval $(0.5 \leq \sigma \leq 5)$ the device operates as projected. For this input case when the disorders are added in the first line, the same considerations are valid. For the second line, only disorders with $\sigma = [15, 20]$ can produce output transmission that infringe the lower tolerance value of the input case. Modifications in the second line with $(0.5 \leq \sigma \leq 10)$ can be neglected.

It can be said with 95% of confidence level that the disorders application in the third line not affect the correct function of the device.

Table 5.8 explains the mean, standard deviation and the confidence interval, computed with 95% of confidence level, for the $(1, 1)$ input case, lines 1,2,3 and for all cylinders.

For the input $(1, 1)$ when all cylinders are modified with $\sigma = [15, 20]$ the upper boundary of tolerance is infringed as a result of a high standard deviation, due to low transmission values obtained and the confidence interval includes 0.17. Thus, with 95% of confidence level, it can be said that the system probably does not operate as projected. Moreover, when the disorders are added using $(0.5 \leq \sigma \leq 10)$ the device operates as expected. If the disorders are added in the first line the same considerations are valid.

For the second and third lines, modifications with $(0.5 \leq \sigma \leq 20)$ the upper limit of tolerance is not infringed, thus the correct operation of the device is achieved.

As demonstrated above, the cylinders of the first line have greater effect in the performance of the device by the reason that they are closer to the waveguide. Then, six regions are analysed to establish what of them have greatest effect in the device performance, as illustrated in Figure 5.9.

The first region, in yellow, is formed by the nine cylinders of the first input and the fourteen of the second input of the waveguide. The second, in red, by the cylinders that form the inclination of the inputs waveguide. The third, in gray, by the sixteen cylinders of the output. The fourth, in green, is composed by the four cylinders that form the edge of the second input waveguide. The fifth, in blue, is formed by the four

		(1,1)					
		σ					
Region		0.50	1.00	5.00	10.0	15.0	20.0
All	Mean	0.066	0.066	0.069	0.079	0.105	0.194
	Std	0.001	0.002	0.012	0.026	0.059	0.200
	CI	**0.064**	**0.061**	0.045	0.027	**-0.010**	**-0.199**
		0.069	**0.071**	0.093	0.132	**0.221**	**0.587**
Line 1	Mean	0.066	0.066	0.070	0.080	0.109	0.246
	Std	0.001	0.002	0.011	0.026	0.077	0.209
	CI	**0.063**	**0.062**	0.047	0.028	**-0.042**	**-0.164**
		0.069	**0.070**	0.093	0.132	**0.262**	**0.656**
Line 2	Mean	0.066	0.066	0.066	0.068	0.067	0.073
	Std	0.000	0.000	0.000	0.002	0.003	0.045
	CI	**0.066**	**0.066**	**0.065**	0.063	0.059	-0.015
		0.066	**0.067**	**0.068**	0.072	0.074	0.162
Line 3	Mean	0.066	0.066	0.066	0.066	0.066	0.067
	Std	0.000	0.000	0.000	0.000	0.001	0.002
	CI	**0.066**	**0.066**	**0.066**	**0.066**	**0.064**	0.061
		0.066	**0.066**	**0.066**	**0.066**	**0.067**	0.072

Table 5.8: Simulation results for the modifications of all cylinders and the first three lines for the XOR device and (1,1) input case. Std is the standard deviation and CI the confidence interval.
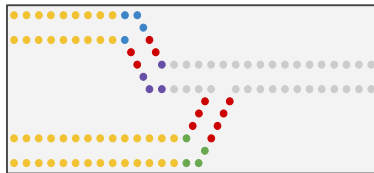
Figure 5.9: Regions analysed for the XOR device.

cylinders that form the edge of the first input. Finally, the sixth region, in purple, is formed by the four cylinders of the inputs waveguide intersection. The results for these regions are shown in Table 5.9.

It is important to note that in average the transmission results are close to the value when the first line is analysed completely. The region with greater impact for the input case $(0, 1)$, as shown in Figure 5.10b, is the first. For the $(1, 0)$ input case the region three, as illustrated in Figure 5.10c, and for the input case $(1, 1)$ the first region, as illustrated in Figure 5.10d.

Figure 5.10a shows the normalized average of the XOR logic gate. As can been observed, the first region has greater effect for this device by the reason that it is projected with triangular lattice and the periodicity in the straight lines can be easily

		(0,1)	(1,0)	(1,1)
		σ	σ	σ
Region		**20.0**	**20.00**	**20.0**
1	**Mean**	0.284	0.775	0.219
	Std	0.129	0.239	0.210
	CI	**0.031**	**0.305**	**-0.193**
		0.537	**1.244**	**0.632**
2	**Mean**	0.293	0.733	0.124
	Std	0.118	0.189	0.139
	CI	**0.061**	**0.361**	**-0.149**
		0.525	**1.105**	**0.398**
3	**Mean**	0.348	0.694	0.083
	Std	0.119	0.234	0.108
	CI	**0.113**	**0.234**	**-0.129**
		0.583	**1.155**	**0.297**
4	**Mean**	0.295	0.851	0.120
	Std	0.066	0.076	0.167
	CI	**0.165**	**0.701**	**-0.207**
		0.425	**1.001**	**0.449**
5	**Mean**	0.319	0.811	0.078
	Std	0.099	0.086	0.021
	CI	**0.125**	**0.642**	**0.036**
		0.514	**0.979**	**0.119**
6	**Mean**	0.293	0.839	0.083
	Std	0.084	0.029	0.040
	CI	**0.126**	**0.781**	**0.004**
		0.459	**0.897**	**0.162**

Table 5.9: Simulations results of the first line regions for the XOR device. Std is the standard deviation and CI the confidence interval.

broken.

5.2.3 Majority Gate

For the Majority logic gate the lines to be analysed are detailed in Figure 5.11. The lower boundary of the tolerance to consider an error is 0.75 for the cases when the logical output is 1 and the upper limit is 0.45 for the cases when the logical output is 0.

As described in the Section 5.1.1 the output transmission for the inputs cases (0,1,0),(0,0,1),(1,0,0) are the same. The mean, standard deviation and the confidence interval, computed with 95% of confidence level, are described in Table 5.10 for the (0,1,0) and (0,1,1) input cases, lines 1,2,3 and for all cylinders.
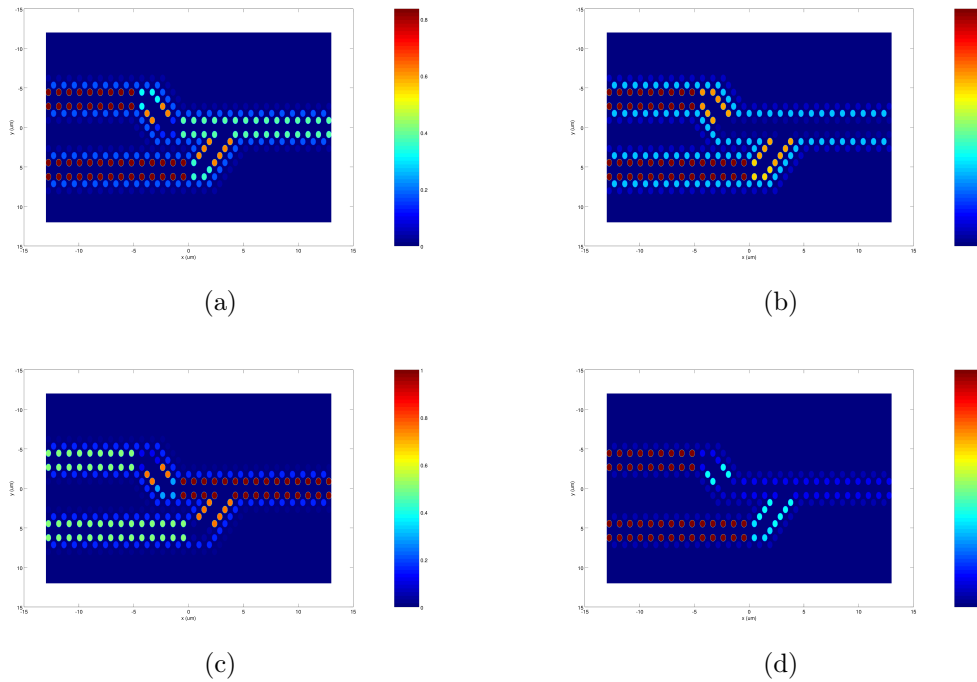
Figure 5.10: Regions effect for the XOR device. (a) Normalized average. (b) Input case (0,1). (C) Input case (1,0). (d) Input case (1,1).
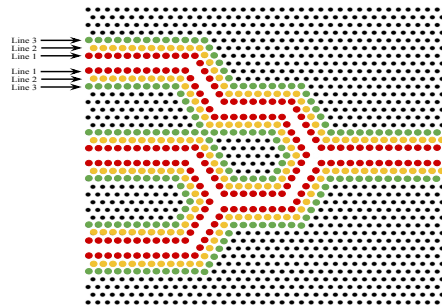
Figure 5.11: Lines analysed for the Majority logic device.

For the input (0,1,0) when all cylinders are modified with $\sigma = [15, 20]$ the upper boundary of tolerance is infringed as a result of a high standard deviation, due to low transmission values obtained and the confidence interval includes 0.45. Thus, with 95% of confidence level, it can be said that the system probably operates unexpectedly. On the other hand, when the disorders are added using $(0.5 \leq \sigma \leq 5)$ the device operates as expected. If the disorders are added in the first line the same considerations are valid.

For the second line, only disorders with $\sigma = 20$ can produce output transmission that infringe the upper tolerance value. On the other hand, modifications with $(0.5 \leq$

		(0,1,0)						(0,1,1)					
		σ						σ					
Region		0.50	1.00	5.00	10.0	15.0	20.0	0.50	1.00	5.00	10.0	15.0	20.0
All	Mean	0.319	0.319	0.318	0.309	0.297	0.228	0.874	0.872	0.871	0.848	0.586	0.362
	Std	0.002	0.005	0.030	0.055	0.143	0.236	0.005	0.011	0.049	0.125	0.172	0.298
	CI	**0.314**	**0.308**	0.258	0.200	0.015	**-0.235**	**0.863**	**0.850**	0.774	0.601	0.247	**-0.222**
		0.325	**0.330**	0.378	0.418	0.580	**0.692**	**0.884**	**0.893**	0.967	1.094	0.925	**0.946**
Line 1	Mean	0.319	0.319	0.319	0.310	0.289	0.222	0.881	0.881	0.879	0.875	0.550	0.363
	Std	0.002	0.005	0.028	0.064	0.107	0.164	0.004	0.009	0.049	0.087	0.190	0.210
	CI	**0.314**	**0.307**	0.263	0.183	0.078	**-0.099**	0.872	0.862	0.781	0.703	0.177	**-0.049**
		0.323	**0.330**	0.374	0.437	0.499	**0.543**	0.890	0.899	0.976	1.046	0.923	**0.775**
Line 2	Mean	0.319	0.319	0.319	0.317	0.315	0.301	0.881	0.881	0.881	0.878	0.874	0.775
	Std	0.001	0.001	0.002	0.002	0.041	0.127	0.000	0.001	0.001	0.005	0.060	0.149
	CI	**0.317**	**0.317**	**0.315**	0.313	0.235	0.052	**0.881**	**0.879**	**0.879**	0.868	0.756	0.483
		0.321	**0.321**	**0.323**	0.321	0.395	0.550	**0.881**	**0.883**	**0.883**	0.888	0.992	1.067
Line 3	Mean	0.319	0.319	0.319	0.319	0.317	0.312	0.881	0.881	0.881	0.879	0.876	0.863
	Std	0.000	0.000	0.000	0.000	0.002	0.006	0.000	0.000	0.000	0.001	0.002	0.005
	CI	**0.319**	**0.319**	**0.319**	**0.319**	0.313	0.300	**0.881**	**0.881**	**0.881**	**0.877**	0.872	0.853
		0.319	**0.319**	**0.319**	**0.319**	0.321	0.324	**0.881**	**0.881**	**0.881**	**0.881**	0.880	0.873

Table 5.10: Simulation results for the modifications of all cylinders and the first three lines for the Majority device and (0,1,0) and (0,1,1) input cases. Std is the standard deviation and CI the confidence interval.

$\sigma \leq 15$) not infringe the upper boundary of tolerance and the device operates correctly.

Finally, it can be said with 95% of confidence level that the cylinders of the third line not affect the correct operation of the device applying disorders in the interval $(0.5 \leq \sigma \leq 20)$.

For the input (0,1,1) when all cylinders are modified with $\sigma = [10, 15, 20]$ the lower boundary of tolerance is infringed as a result of a high standard deviation, due to low transmission values obtained and the confidence interval includes 0. Thus, with 95% of confidence level, it can be said that the system probably operates unexpectedly. In contrast, when the disorders are added using $(0.5 \leq \sigma \leq 5)$ the device operates as projected. If the disorders are added in the first line the same considerations are valid.

For the second line, only disorders with $\sigma = 20$ can produce output transmission that infringe the lower tolerance value. Moreover, modifications with $(0.5 \leq \sigma \leq 15)$ not infringe the upper boundary of tolerance and the device operates correctly.

The disorders applied in the third line can be neglected because the device performance is not affected.

The simulation results shown that the output transmission for the majority logic device when the inputs are (1,0,1) and (1,1,0) are equal. Then, Table 5.11 displays

the results for the (1,0,1) and (1,1,1) input cases, when all cylinders, first, second and third lines are modified.

		(1,0,1)						(1,1,1)					
		σ						σ					
Region		0.50	1.00	5.00	10.0	15.0	20.0	0.50	1.00	5.00	10.0	15.0	20.0
All	Mean	0.952	0.951	0.948	0.932	0.631	0.328	1.000	1.000	1.000	0.985	0.896	0.430
	Std	0.003	0.006	0.029	0.063	0.118	0.224	0.004	0.009	0.042	0.092	0.179	0.325
	CI	**0.945**	**0.938**	0.891	0.808	0.399	**-0.111**	**0.992**	**0.984**	0.921	0.803	0.544	**-0.206**
		0.958	**0.963**	1.004	1.056	0.863	**0.768**	**1.009**	**1.019**	1.088	1.167	1.248	**1.067**
Line 1	Mean	0.952	0.951	0.950	0.946	0.694	0.332	1.000	1.000	0.985	0.983	0.888	0.484
	Std	0.004	0.005	0.032	0.066	0.122	0.258	0.005	0.006	0.041	0.073	0.231	0.428
	CI	**0.944**	**0.940**	0.886	0.815	0.455	**-0.172**	**0.990**	**0.988**	0.903	0.840	0.434	**-0.354**
		0.959	**0.961**	1.013	1.076	0.934	**0.838**	**1.012**	**1.014**	1.067	1.126	1.341	**1.323**
Line 2	Mean	0.952	0.952	0.951	0.948	0.891	0.884	1.000	1.000	0.984	0.978	0.922	0.885
	Std	0.001	0.001	0.002	0.002	0.041	0.127	0.000	0.001	0.001	0.005	0.060	0.149
	CI	**0.950**	**0.950**	**0.947**	**0.944**	0.811	0.635	**1.000**	**0.998**	**0.982**	**0.968**	0.804	0.593
		0.954	**0.954**	**0.955**	**0.952**	0.971	1.133	**1.000**	**1.002**	**0.986**	**0.988**	1.040	1.177
Line 3	Mean	0.952	0.952	0.952	0.951	0.946	0.923	1.000	1.000	1.000	0.989	0.983	0.974
	Std	0.000	0.000	0.000	0.000	0.002	0.006	0.000	0.000	0.000	0.001	0.002	0.005
	CI	0.952	0.952	0.952	0.951	0.942	0.911	1.000	1.000	1.000	0.987	0.979	0.964
		0.952	0.952	0.952	0.951	0.950	0.935	1.000	1.000	1.000	0.991	0.987	0.984

Table 5.11: Simulation results for the modifications of all cylinders and the first three lines for the Majority device and (1,0,1) and (1,1,1) input cases. Std is the standard deviation and CI the confidence interval.

For the input (1,0,1) when all cylinders are modified with $\sigma = [15, 20]$ the lower boundary of tolerance is infringed as a result of a high standard deviation, due to low transmission values obtained and the confidence interval includes 0.75. Thus, with 95% of confidence level, it can be said that the system probably operates unexpectedly. In contrast, when the disorders are added using ($0.5 \leq \sigma \leq 10$) the device operates as projected. If the disorders are added in the first line the same considerations are valid.

For the second line, only disorders with $\sigma = 20$ can produce output transmission that infringe the lower tolerance value. Moreover, modifications with ($0.5 \leq \sigma \leq 15$) not infringe the upper boundary of tolerance and the device operates correctly.

The disorders are applied in the third line are insignificant because the device performance is not affected.

For the input (1,1,1) when all cylinders are modified with $\sigma = [15, 20]$ the lower boundary of tolerance is infringed as a result of a high standard deviation, due to low transmission values obtained and the confidence interval includes 0.75. Thus, with 95% of confidence level, it can be said that the system probably operates unexpectedly. On

the other hand, when the disorders are added using $(0.5 \leq \sigma \leq 10)$ the device operates as projected. If the disorders are added in the first line the same considerations are valid.

For the second line, only disorders with $\sigma = 20$ can produce output transmission that infringe the lower tolerance value. Moreover, modifications with $(0.5 \leq \sigma \leq 15)$ do not infringe the upper boundary of tolerance and the device operates correctly.

The disorders applied in the third line can be neglected due to the fact that the device performance is not affected.

Six regions of the first line are analysed to establish their effect in the device performance, as illustrated in Figure 5.12.
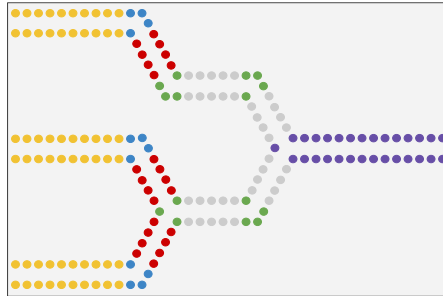
Figure 5.12: Regions analysed for the Majority logic device.

The first region, in yellow, is formed by the first nine cylinders of the waveguide input. The second, in red, by the four cylinders that form the inclination of the waveguide inputs. The third, in gray, by the cylinders of that form the waveguide path intersection. The fourth, in purple, by the cylinders that form the output. The fifth, in blue, is composed by the four cylinders that form the edge of the waveguide and the sixth region is formed by the cylinders of the four intersections, in green. The simulations results for these regions are shown in Table 5.12.

It is important to note that in average the transmission results are close to the value when the first line is analysed completely. The region with greater impact for the input case (0,1,0) is the third, as shown in, as shown in Figure 5.13b. For the input case (0,1,1) the third region, as illustrated in Figure 5.13c. For the (1,0,1) input case the region three, as illustrated in Figure 5.13d and for the input case (1,1,1) the first region, as shown in Figure 5.13e.

Figure 5.13a shows the normalized average of the Majority logic gate, as can been observed, the third region has greater effect for this device by the reason that it is projected with triangular lattice and the periodicity in the straight lines can be easily broken.

		(0,1,0)	(0,1,1)	(1,0,1)	(1,1,1)
		σ	σ	σ	σ
Region		**20.0**	**20.0**	**20.0**	**20.0**
1	**Mean**	0.289	0.385	0.578	0.503
	Std	0.061	0.021	0.082	0.077
	CI	0.169	**0.344**	**0.417**	**0.352**
		0.409	**0.426**	**0.739**	**0.654**
2	**Mean**	0.274	0.423	0.531	0.628
	Std	0.078	0.027	0.052	0.093
	CI	**0.121**	**0.370**	**0.429**	**0.446**
		0.427	**0.476**	**0.633**	**0.810**
3	**Mean**	0.267	0.568	0.380	0.540
	Std	0.069	0.030	0.023	0.048
	CI	0.132	**0.509**	**0.335**	**0.446**
		0.402	**0.627**	**0.425**	**0.634**
4	**Mean**	0.232	0.391	0.358	0.519
	Std	0.086	0.023	0.039	0.093
	CI	0.063	**0.346**	**0.282**	**0.337**
		0.401	**0.436**	**0.434**	**0.701**
5	**Mean**	0.261	0.437	0.459	0.571
	Std	0.043	0.079	0.068	0.085
	CI	0.177	**0.282**	**0.326**	**0.404**
		0.345	**0.592**	**0.592**	**0.738**
6	**Mean**	0.287	0.553	0.481	0.631
	Std	0.034	0.170	0.036	0.058
	CI	0.220	**0.220**	**0.410**	**0.517**
		0.354	**0.886**	**0.552**	**0.745**

Table 5.12: Simulations results of the first line regions for the Majority device. Std is the standard deviation and CI the confidence interval.

5.2.4 Feynman Gate

For the Feynman logic device the lines to be analysed are detailed Figure 5.14. The lower boundary of the tolerance to consider an error is 0.3 for the cases when the logical output is 1 and the upper limit is 0.2 for the cases when the logical output is 0.

The mean, standard deviation and the confidence interval, computed with 95% of confidence level, are explained in Table 5.13 for the (0,1) input case, lines 1,2,3 and for all cylinders.

As can been observed for the (0,1) and output X, similarly to the other logic gates when modifications are added to all cylinders and the first line with $\sigma = [15, 20]$ infringe the tolerance limit defined. Only the disorders with $\sigma = 20$ infringe the tolerance limit in the second line. The disorders added in the third line can be neglected.

(a)

(b)

(c)

(d)

(e)

Figure 5.13: Regions effect for the Majority device. (a) Normalized average. (b) Input case (0,1,0). (c) Input case (0,1,1). (d) Input case (1,0,1). (e) Input case (1,1,1).

Figure 5.14: Lines analysed for the Feynman logic device.

For the the (0,1) and output Y, disorders in the order of $\sigma = [10, 15, 20]$ affect the device performance when are added in the first line and to all cylinders. For the second line, disorder with $\sigma = [15, 20]$ generates unexpectedly behaviours in the device. The modifications added in the third line can be neglected.

		(0,1)-x						(0,1)-y					
		σ						σ					
Region		0.50	1.00	5.00	10.0	15.0	20.0	0.50	1.00	5.00	10.0	15.0	20.0
All	Mean	0.107	0.107	0.103	0.101	0.113	0.133	0.503	0.503	0.501	0.484	0.396	0.289
	Std	0.002	0.002	0.012	0.028	0.050	0.136	0.006	0.006	0.034	0.075	0.099	0.254
	CI	**0.102**	**0.102**	0.078	0.046	0.015	**-0.134**	0.490	0.490	0.433	0.336	0.201	**-0.208**
		0.112	**0.112**	0.128	0.156	0.211	**0.400**	0.515	0.515	0.568	0.631	0.591	**0.787**
Line 1	Mean	0.107	0.107	0.106	0.102	0.124	0.137	0.503	0.502	0.502	0.464	0.397	0.258
	Std	0.001	0.002	0.008	0.013	0.096	0.121	0.002	0.005	0.007	0.042	0.087	0.144
	CI	0.105	0.103	0.090	0.077	-0.0645	-0.100	**0.499**	**0.492**	0.488	0.382	0.226	**-0.024**
		0.109	0.111	0.121	0.127	0.312	0.374	**0.507**	**0.512**	0.516	0.546	0.568	**0.540**
Line 2	Mean	0.107	0.107	0.107	0.103	0.101	0.085	0.503	0.503	0.503	0.501	0.478	0.461
	Std	0.001	0.001	0.002	0.002	0.041	0.127	0.000	0.001	0.001	0.005	0.060	0.149
	CI	**0.105**	**0.105**	**0.103**	**0.099**	0.021	**-0.164**	0.503	**0.501**	**0.501**	**0.491**	0.360	0.169
		0.109	**0.109**	**0.111**	**0.107**	0.181	**0.334**	0.503	**0.505**	**0.505**	**0.511**	0.596	0.753
Line 3	Mean	0.107	0.107	0.107	0.105	0.104	0.101	0.503	0.503	0.503	0.503	0.501	0.497
	Std	0.000	0.000	0.000	0.002	0.004	0.006	0.000	0.000	0.000	0.001	0.002	0.005
	CI	**0.107**	**0.107**	**0.107**	**0.101**	0.096	0.089	**0.503**	**0.503**	**0.503**	**0.501**	0.497	0.487
		0.107	**0.107**	**0.107**	**0.109**	0.112	0.113	**0.503**	**0.503**	**0.503**	**0.505**	0.505	0.507

Table 5.13: Simulation results for the modifications of all cylinders and the first three lines for the Feynman device and (0,1) input case. Std is the standard deviation and CI the confidence interval.

Table 5.14 details the simulation results for the input (1,0), when all cylinders are modified and the first, second and third lines. The numbers in red represent the cases when the tolerance value is infringed, in yellow when are close to the limits and when the expected value is close to the real transmission in green.

For the (1,0) and output X, when modifications are added to all cylinders and the first line with $\sigma = [15, 20]$ infringe the tolerance limit defined. Only the disorders with $\sigma = 20$ infringe the tolerance limit in the second line. The disorders added in the third line can be neglected.
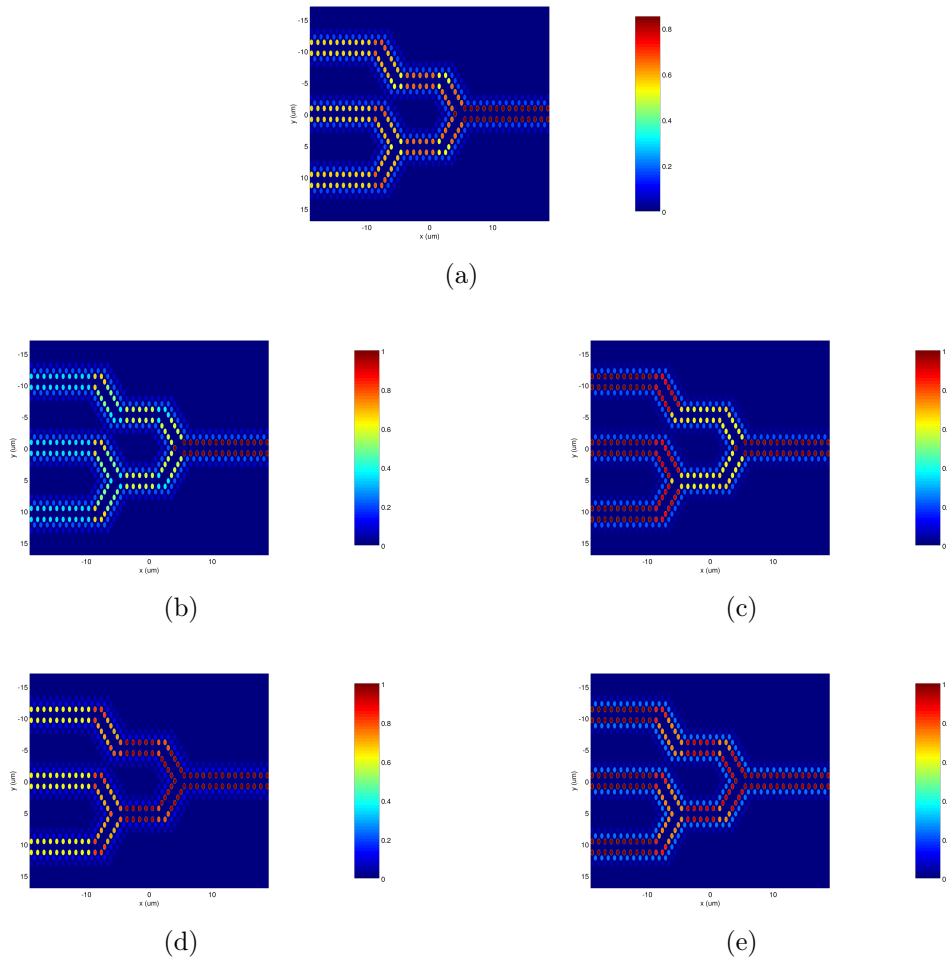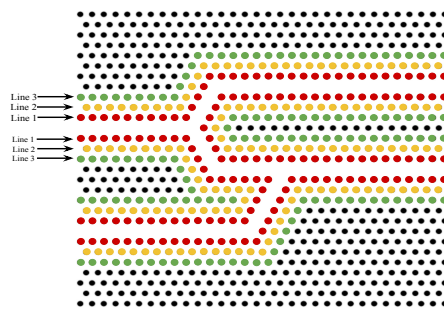
For the the (1,0) and output Y, disorders in the order of $\sigma = [10, 15, 20]$ affect the device performance when are added in the first line and to all cylinders. For the second line, disorder with $\sigma = [10, 15, 20]$ generates unexpectedly behaviours in the device. The modifications added in the third line can be neglected.

Table 5.15 explains the simulations result for the (1,1) input case, when all cylinders, the first, second and third lines are modified. The numbers in red represent the cases when the tolerance value is infringed, in yellow when are close to the limits and when the expected value is close to the real transmission in green.

For the (1,1) and output X, when modifications are added to all cylinders with

| | | (1,0)-x | | | | | | (1,0)-y | | | | | |
| | | σ | | | | | | σ | | | | | |
Region		0.50	1.00	5.00	10.0	15.0	20.0	0.50	1.00	5.00	10.0	15.0	20.0
All	Mean	0.451	0.451	0.448	0.445	0.440	0.427	0.398	0.397	0.395	0.391	0.387	0.228
	Std	0.002	0.005	0.026	0.062	0.152	0.265	0.002	0.004	0.021	0.041	0.090	0.167
	CI	**0.445**	**0.441**	0.396	0.323	0.141	**-0.093**	**0.393**	**0.389**	0.352	0.309	0.210	**-0.098**
		0.456	**0.461**	0.499	0.566	0.738	**0.948**	**0.402**	**0.405**	0.437	0.472	0.563	**0.556**
Line 1	Mean	0.451	0.451	0.446	0.445	0.423	0.391	0.398	0.398	0.383	0.374	0.361	0.238
	Std	0.002	0.004	0.005	0.008	0.121	0.254	0.003	0.007	0.014	0.052	0.112	0.234
	CI	**0.447**	**0.443**	**0.436**	0.429	0.186	-0.107	**0.392**	**0.384**	0.356	0.272	0.141	**-0.221**
		0.455	**0.459**	**0.456**	0.461	0.660	0.889	**0.404**	**0.412**	0.410	0.476	0.581	**0.697**
Line 2	Mean	0.451	0.451	0.450	0.448	0.427	0.425	0.398	0.398	0.396	0.384	0.381	0.351
	Std	0.000	0.001	0.004	0.005	0.035	0.115	0.000	0.002	0.003	0.006	0.051	0.133
	CI	**0.451**	**0.449**	**0.442**	0.438	0.358	0.200	0.398	0.394	0.390	0.372	0.281	0.091
		0.451	**0.453**	**0.458**	0.458	0.496	0.650	0.398	0.402	0.402	0.396	0.481	0.611
Line 3	Mean	0.451	0.451	0.451	0.451	0.448	0.447	0.398	0.398	0.398	0.398	0.395	0.392
	Std	0.000	0.000	0.000	0.001	0.003	0.004	0.000	0.000	0.000	0.002	0.004	0.008
	CI	**0.451**	**0.451**	**0.451**	**0.449**	0.442	0.439	**0.398**	**0.398**	**0.398**	**0.394**	0.387	0.376
		0.451	**0.451**	**0.451**	**0.453**	0.454	0.455	**0.398**	**0.398**	**0.398**	**0.402**	0.403	0.408

Table 5.14: Simulation results for the modifications of all cylinders and the first three lines for the Feynman device and (1,0) input case. Std is the standard deviation and CI the confidence interval.

$\sigma = [10, 15, 20]$ infringe the tolerance limit defined. Modifications with $\sigma = [15, 20]$ and $\sigma = 20$ for the first line and for the second line, respectively, infringe the tolerance limit. The disorders added in the third line can be neglected.

For the the (1,1) and output Y, disorders in the order of $\sigma = 20$ to all cylinders and $\sigma = [15, 20]$ in the first line affect the device performance. For the second line, disorder with $\sigma = 20$ generates unexpectedly behaviours in the device. The modifications added in the third line can be neglected.

Five regions of the first line are analysed to establish their effect in the device performance, illustrated in Figure 5.15.
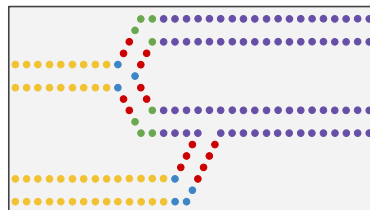

Figure 5.15: Regions analysed for the Feynman logic device.

The first region, in yellow, is formed by the nine cylinders of the first input and

		(1,1)-x						(1,1)-y					
		σ						σ					
Region		0.50	1.00	5.00	10.0	15.0	20.0	0.50	1.00	5.00	10.0	15.0	20.0
All	Mean	0.730	0.731	0.732	0.716	0.669	0.352	0.019	0.019	0.018	0.033	0.052	0.186
	Std	0.002	0.006	0.030	0.073	0.118	0.260	0.001	0.001	0.006	0.026	0.059	0.166
	CI	0.726	0.718	0.672	0.573	0.436	-0.157	0.017	0.016	0.005	-0.018	-0.064	-0.139
		0.735	0.744	0.792	0.859	0.902	0.862	0.021	0.022	0.031	0.085	0.168	0.511
Line 1	Mean	0.730	0.730	0.728	0.719	0.675	0.382	0.019	0.019	0.017	0.028	0.048	0.167
	Std	0.001	0.003	0.007	0.034	0.118	0.267	0.003	0.005	0.007	0.018	0.108	0.195
	CI	0.728	0.724	0.714	0.652	0.444	-0.141	0.013	0.009	0.003	-0.007	-0.164	-0.215
		0.732	0.736	0.742	0.786	0.906	0.905	0.025	0.029	0.031	0.063	0.260	0.549
Line 2	Mean	0.730	0.730	0.730	0.726	0.715	0.672	0.019	0.019	0.019	0.014	0.010	0.045
	Std	0.000	0.003	0.004	0.007	0.021	0.108	0.000	0.002	0.005	0.006	0.009	0.122
	CI	0.730	0.724	0.722	0.712	0.674	0.460	0.019	0.015	0.009	0.002	-0.008	-0.194
		0.730	0.736	0.738	0.740	0.756	0.884	0.019	0.023	0.029	0.026	0.028	0.284
Line 3	Mean	0.730	0.730	0.730	0.730	0.728	0.749	0.019	0.019	0.019	0.019	0.014	0.012
	Std	0.000	0.000	0.000	0.002	0.003	0.006	0.000	0.000	0.000	0.002	0.005	0.006
	IC	0.730	0.730	0.730	0.726	0.722	0.737	0.019	0.019	0.019	0.015	0.004	0.000
		0.730	0.730	0.730	0.734	0.734	0.761	0.019	0.019	0.019	0.023	0.024	0.024

Table 5.15: Simulation results for the modifications of all cylinders and the first three lines for the Feynman device and (1,1) input case. Std is the standard deviation and CI the confidence interval.

the fourteen of the second input of the waveguide. The second, in red, by the cylinders that form the inclination of the inputs waveguide. The third, in purple, by the cylinders that form the outputs path. The fourth, in blue, is composed by the cylinders of the first intersections and the fifth region, in green, is formed by the cylinders that form the edges to the output waveguide. The simulations result of the these regions are shown in Table 5.16.

As can been observed in average the transmission results are close to the value when the first line is analysed completely.

The region with greater influence for the input case (0,1) is the first, as shown in Figure 5.16c and Figure 5.16d, for the input case (1,0) the region 3, as illustrated in Figure 5.16e and Figure 5.16f. For the input case (1,1) the region 1, as shown in Figure 5.16g and Figure 5.16h.

Figure 5.16a and Figure 5.16b display the normalized average for output X and Y respectively. The first region has greater effect for this device by the reason that it is projected with triangular lattice and the periodicity in the straight lines can be easily broken.

		(0,1)-x	(0,1)-y	(1,0)-x	(1,0)-y	(1,1)-x	(1,1)-y
		σ	σ	σ	σ	σ	
Region		**20.0**	**20.0**	**20.0**	**20.0**	**20.0**	**20.0**
1	**Mean**	0.132	0.293	0.365	0.319	0.358	0.157
	Std	0.032	0.083	0.021	0.069	0.089	0.023
	CI	0.069	0.131	0.324	0.184	0.184	0.112
		0.195	0.456	0.406	0.454	0.532	0.202
2	**Mean**	0.113	0.310	0.341	0.287	0.393	0.143
	Std	0.045	0.073	0.067	0.024	0.078	0.087
	CI	0.025	0.167	0.210	0.240	0.240	-0.028
		0.201	0.453	0.472	0.334	0.546	0.314
3	**Mean**	0.084	0.376	0.325	0.279	0.412	0.135
	Std	0.067	0.080	0.078	0.035	0.027	0.066
	CI	-0.047	0.219	0.172	0.210	0.359	0.006
		0.215	0.533	0.478	0.348	0.465	0.264
4	**Mean**	0.119	0.316	0.378	0.323	0.442	0.078
	Std	0.016	0.056	0.092	0.076	0.063	0.075
	CI	0.088	0.206	0.198	0.174	0.319	-0.069
		0.150	0.426	0.558	0.472	0.565	0.225
5	**Mean**	0.083	0.389	0.359	0.298	0.451	0.068
	Std	0.025	0.047	0.089	0.037	0.047	0.072
	CI	0.034	0.297	0.185	0.225	0.359	-0.073
		0.132	0.481	0.533	0.371	0.543	0.209

Table 5.16: Simulation results of the first line regions for the Feynman device. Std is the standard deviation and CI the confidence interval.

5.3 Cascading of Logic Gates

The photonic logic devices studied in this work are novel and have a great potential to be applied in future all-optical integrated circuits (AOIC). Still, the development of AOIC faces great challenges, especially for the cascade of logic gates.

      There are two major problems. First, when light beams are injected in inputs (logic 1) they propagate not only to the outputs, but also back to other inputs with logic 0. This feedback signal must be suppressed in order to avoid its propagation to previous gates. Second, due to losses the values at the outputs are weaker than in the inputs. Also, the output of different logic gates presents unequal threshold values. Once an amplifier is created and connected to the output this problem will be solved.
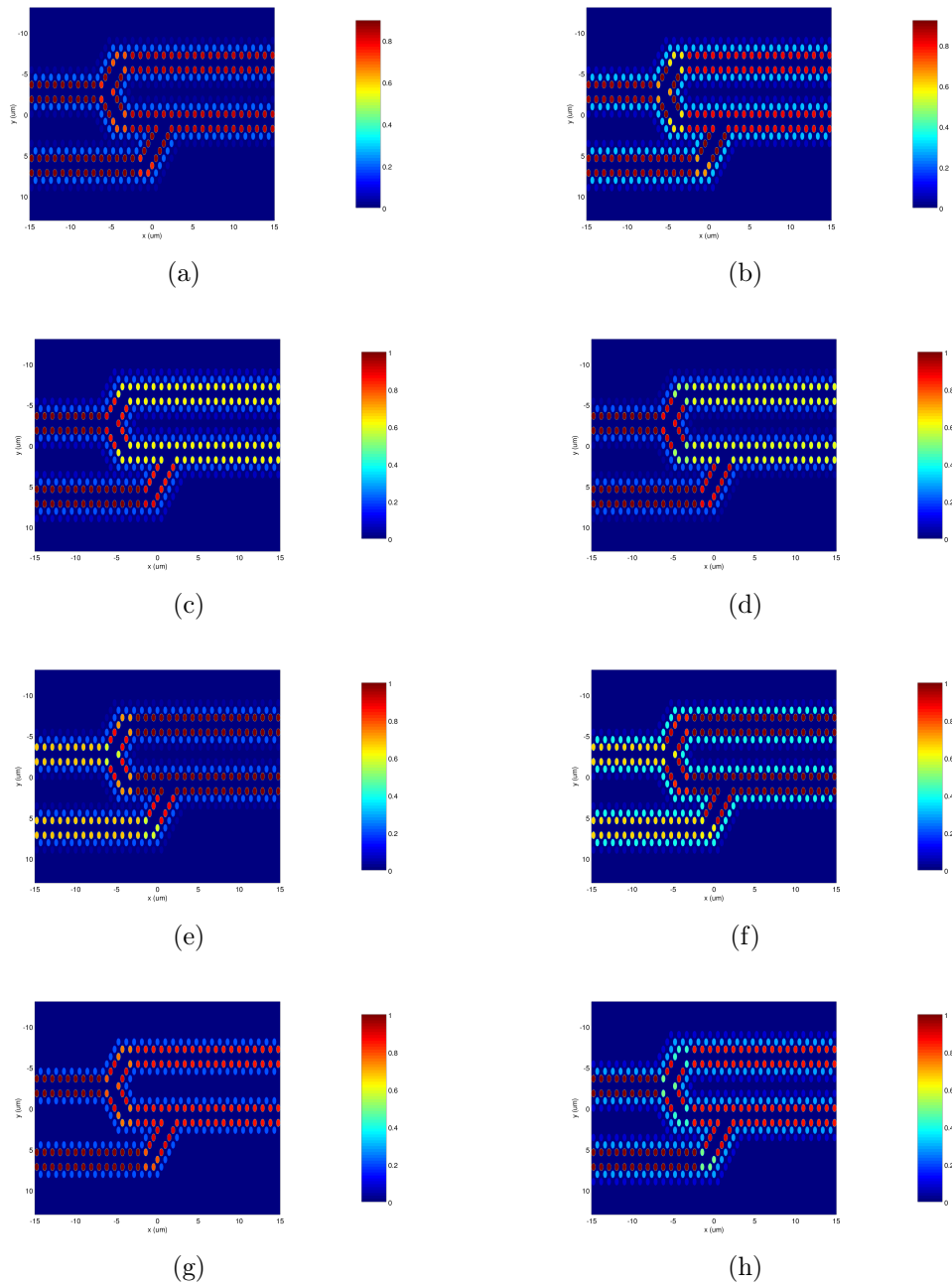
Figure 5.16: Regions effect for the Feynman device. The normalised average for output X (a) and Y (b). Input case (0,1), output X (c) and Y (d). Input case (1,0), output X (e) and Y (f). Input case (1,1), output X (g) and Y (h).

Chapter 6

Conclusions and Future Work

The optimization of semiconductor nanodevices is an important step in the way to develop and discover new optoelectronic devices. Moreover, it is a very difficult process that present several challenges to the scientist. Fortunately, computational techniques can support this kind of process in order to achieve efficient and effective results more quickly.

In this work, an approximate method to achieve automatically the energy-band configuration of superlattices of quantum wells was implemented and used in conjunction with a genetic algorithm to find structures with a desired energy-band configuration. The experimental results demonstrate that the GA is an adequate, effective and efficient computational technique to the optimization of superlattice with central quantum well. The best structures found here have great potential to be grown experimentally in order to develop new optoelectronic devices such as photodetectors.

In addition, two all-optical gates in photonic crystals were proposed: the Majority and the Feynman gates. The majority gate is a compact device that can operate as AND or OR logic gate. Also, it can be used to create simple and optimized logic, such as in other technologies (QCA and SET). The Feynman gate is reversible and can be used to achieve the limits of power consumption in computation. The numerical analysis, using the FDTD method, shows that the logic 0 and 1 are defined as less than 35% and more than 85% of transmission, respectively, for the Majority gate. For the all-optical Feynman gate device, the logic 0 and 1 are defined as less than 10% and more than 40% of transmission, respectively. The devices presented here can be used to design photonic computational circuits. However, this technology introduces new challenges, such as the feedback problem to the inputs and the weaker values at the outputs. Once these problems are solved the cascade of gates will be allowed, enabling the creation of photonic integrated circuits.

A methodology to evaluate the robustness of the logic devices in two-dimensional photonic crystals are applied to these devices. The simulations results show that the first line has the greater effect in the performance on the device, by the reason that it is close to the waveguide. The regions of the first line with great impact in the device operation are the ones formed by straight lines because the periodicity can be easily broken. In general, with 95% of confidence level the logic devices designed with these geometries are robust and can support modifications of about $\pm 40nm$ for a tolerance in the transmission output of ± 0.1. Therefore, the devices studied here have great potential to be grown experimentally.

6.1   Future Work

From this work, many others may arise. It is possible to highlight:

- Applying other computational intelligence techniques to perform the energy-band configuration automatically of the superlattices of quantum wells.

- Consider the calculation of the transmission coefficient under the barriers.

- Evaluate other penalization values and consider the number of discrete energy levels and minibands in the fitness function.

- Try other metaheuristics to optimize superlattices of quantum wells and compare their results with those obtained in this work.

- Perform the experimental growth of the superlattices of quantum wells structures found in this work.

- Evaluate the robustness of other all-optical logic devices in photonic crystals.

- Perform the experimental growth of the all-optical logic devices proposed in this work.

- Use computational optimization techniques to the discovery of new all-optical logic devices.

- Investigate other types of structures and phenomenons in photonic crystals to solve the feedback problem and the cascade of the logic gates.

Bibliography

Cavin, R., Lugli, P., and Zhirnov, V. (2012). Science and engineering beyond Mooreś law. *Proceedings of the IEEE*, 100(Special Centennial Issue):1720–1749. ISSN 0018-9219.

Chen, P. Y., Chen, C. H., Wu, J. S., Wen, H. C., and Wang, W. P. (2007). Optimal design of integrally gated cnt field-emission devices using a genetic algorithm. *Nanotechnology*, 18(39):395203.

Cotta, E., Vilela Neto, O., and da Silva Coelho, F. (2014). Genetic algorithm applied to the optimized project of semiconductor microcavity lasers. In *Microelectronics Technology and Devices (SBMicro), 2014 29th Symposium on*, pages 1–4.

Darwin, C. (1859). On the origins of species by means of natural selection. *London: Murray*, page 247.

Deb, S., Singh, N. B., Sarkar, S. K., and Sarkara, S. K. (2010). Parameter optimization for better quantum well nanostructure based on comparative performance analysis of particle swarm optimization and genetic algorithm. *Journal of Computational and Theoretical Nanoscience*, 7(10):2024–2030.

Degani, M. H. and Maialle, M. Z. (2010). Numerical calculations of the quantum states in semiconductor nanostructures. *Journal of Computational and Theoretical Nanoscience*, 7(2):454–473.

Duan, F. and Guojun, J. (2005). *Introduction to condensed matter physics*, volume 109. World Scientific.

Feichtner, T., Selig, O., Kiunke, M., and Hecht, B. (2012). Evolutionary optimization of optical antennas. *Phys. Rev. Lett.*, 109:127701.

Forestiere, C., Donelli, M., Walsh, G. F., Zeni, E., Miano, G., and Negro, L. D. (2010). Particle-swarm optimization of broadband nanoplasmonic arrays. *Opt. Lett.*, 35(2):133--135.

Fu, Y., Hu, X., and Gong, Q. (2013). Silicon photonic crystal all-optical logic gates. *Physics Letters A*, 377(3-4):329 – 333. ISSN 0375-9601.

Ginzburg, P., Berkovitch, N., Nevet, A., Shor, I., and Orenstein, M. (2011). Resonances on-demand for plasmonic nano-particles. *Nano Letters*, 11(6):2329–2333.

Golberg, D. E. (1989). Genetic algorithms in search, optimization, and machine learning. *Addion wesley*, 1989.

Gossard, A. C. et al. (2000). *Advanced Epitaxy for Future Electronics, Optics, and Quantum Physics:: Seventh Lecture International Science Lecture Series*, volume 7. National Academies Press.

Goudarzi, K., Mir, A., Chaharmahali, I., and Goudarzi, D. (2016). All-optical {XOR} and {OR} logic gates based on line and point defects in 2-d photonic crystal. *Optics and Laser Technology*, 78, Part B:139 – 142. ISSN 0030-3992.

Jain, R. (1991). The art of computer systems performance analysis: techniques for experimental design, measurement, simulation, and modeling. *SIGMETRICS Performance Evaluation Review*, 19:5--11.

Joannopoulos, J. D., Johnson, S. G., Winn, J. N., and Meade, R. D. (2008). *Photonic Crystals: Molding the Flow of Light*. Princeton University Press.

Kasap, S. and Capper, P. (2007). *Materials for Optoelectronics and Photonics*. Springer.

Michalewicz, Z. (2013). *Genetic algorithms+ data structures= evolution programs*. Springer Science & Business Media.

Mitchell, M. (1998). *An introduction to genetic algorithms*. MIT press.

Neamen, D. A. (2003). *Semiconductor Physics and Devices: Basic Principles*. McGraw Hill.

Neto, O. P. V. (2014). Intelligent computational nanotechnology: The role of computational intelligence in the development of nanoscience and nanotechnology. *Journal of Computational and Theoretical Nanoscience*, 11(4):928–944.

Neumann, J. V. (1966). *Theory of Self-Reproducing Automata*. University of Illinois Press, Champaign, IL, USA.

Oskooi, A. F., Roundy, D., Ibanescu, M., Bermel, P., Joannopoulos, J., and Johnson, S. G. (2010). Meep: A flexible free-software package for electromagnetic simulations by the FDTD method. *Computer Physics Communications*, 181(3):687 – 702. ISSN 0010-4655.

Passaro, A., Tanaka, R., Muraro, A., Vieira, G., and Abe, N. (2010). Self-consistent optimization of multi-quantum well structures by a genetic algorithm. *Magnetics, IEEE Transactions on*, 46(8):2759–2762. ISSN 0018-9464.

Rani, P., Kalra, Y., and Sinha, R. (2013). Realization of {AND} gate in y shaped photonic crystal waveguide. *Optics Communications*, 298-299:227 – 231. ISSN 0030-4018.

Rezende, S. M. (2004). *Materiais e dispositivos eletrônicos*. Editora Livraria da Física.

Singulani, A. P., Neto, O. P. V., Pacheco, M. C. A., Vellasco, M. B., Pires, M. P., and Souza, P. L. (2008). Computational intelligence applied to the growth of quantum dots. *Journal of Crystal Growth*, 310(23):5063 – 5065. ISSN 0022-0248. The Fourteenth International conference on Metalorganic Vapor Phase EpitaxThe 14th International conference on Metalorganic Vapor Phase Epitax.

Yang, Y.-P., Lin, K.-C., Yang, I.-C., Lee, K.-Y., Lin, Y.-J., Lee, W.-Y., and Tsai, Y.-T. (2013). All-optical photonic crystal {AND} gate with multiple operating wavelengths. *Optics Communications*, 297:165–168. ISSN 0030-4018.

Younis, R., Areed, N., and Obayya, S. (2014). Fully integrated and and or optical logic gates. *Photonics Technology Letters, IEEE*, 26(19):1900–1903. ISSN 1041-1135.

Zeng, S., Zhang, Y., Li, B., and Pun, E. Y.-B. (2010). Ultrasmall optical logic gates based on silicon periodic dielectric waveguides. *Photonics and Nanostructures - Fundamentals and Applications*, 8(1):32 – 37. ISSN 1569-4410.

Appendix A

Publications

A.1 Published

- Pedraza Caballero, L.; Vasco, J.; Guimaraes, P. and Vilela Neto, O. (2015). All-optical majority and feynman gates in photonic crystals. In *Microelectronics Technology and Devices (SBMicro), 2015 30th Symposium on,* pp. 1-4.

A.2 In Production

- Pedraza Caballero, L.; Vasco, J.; Guimaraes, P. and Vilela Neto, O. (2016). Robustness Analysis of All-Optical Logic Gate.
  To be submitted to a journal.

- Pedraza Caballero, L.; Maialle M. and Vilela Neto, O. (2016). Genetic Algorithm Applied to Optimization of Superlattices of Quantum Wells.
  To be submitted to a conference.

Appendix B

SPQW Online Simulator

Superlattice of quantum wells online simulator is a web tool developed in this work to simulate these structure, available at http://www.nanocomp.dcc.ufmg.br/applications/spqws/. As shown in the Figure B.1, this tool is composed of two main modules, to known: Projects and Simulator.
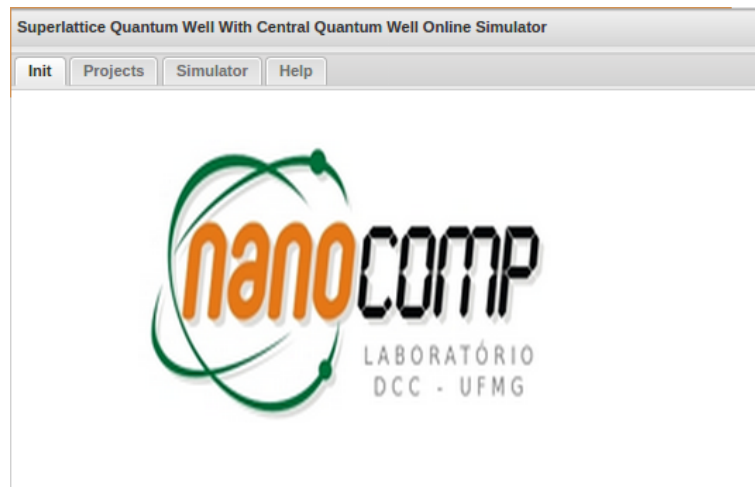
Figure B.1: Init page of SPQW online Simulator.

The simulator module is illustrated in Figure B.2. This module is divided into three sections.

The first section capture the parameters to perform and save the simulation. The second section is an area to view and interact with the coefficient transmission plot. This area have same particular functionalities execute with the commands explained bellow:
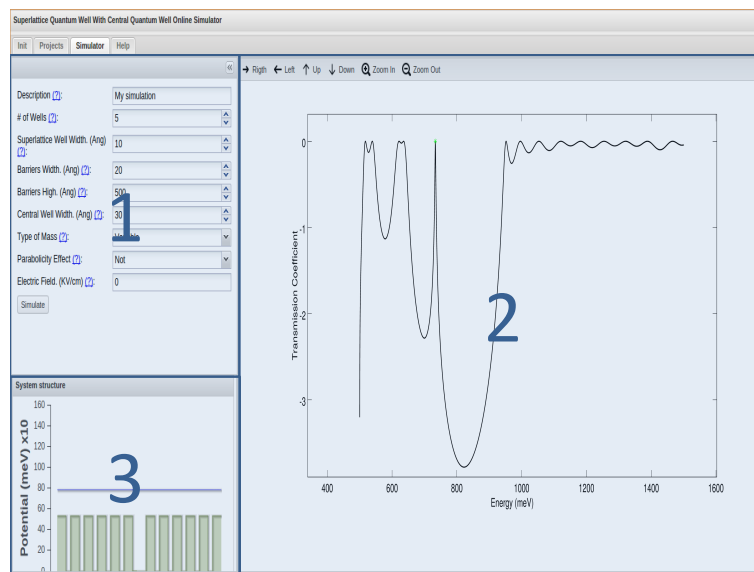
- Scroll for zoom in, zoom out

Figure B.2: Simulator module of the SPQW online simulator.

- Alt + Scroll to right and left

- Shift + Scroll to up and down

- Ctrl + Click to add/delete a peak

- Shift + Click to add/delete the begin of miniband

- Ctrl + Shift + Click to add/delete the end of miniband

The third section is an area exhibiting the energy-band configuration of the simulated structure.

The Projects, shown in Figure B.3 is composed of the history simulations section, plot section and the result simulation section, as shown in figure. It is important to remark that the history simulation section, displayed the all simulations performed in the tool.
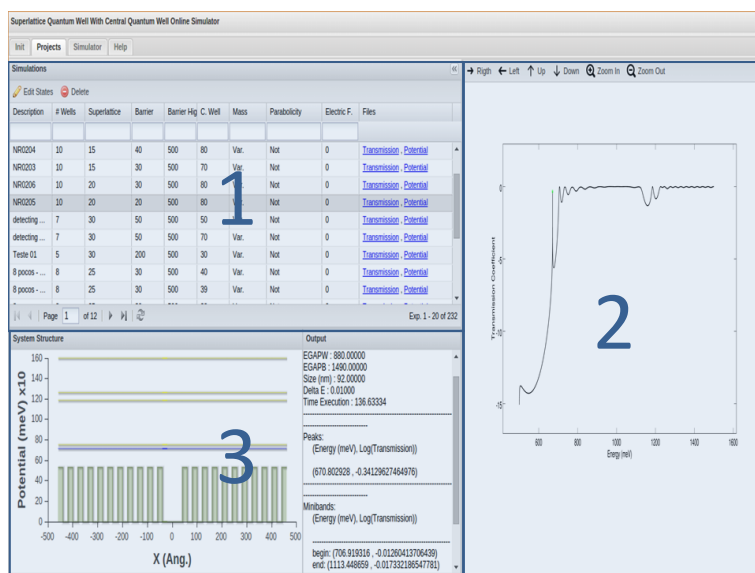
Figure B.3: Projects module of the SPQW online simulator.

Appendix C

Superlattices of Quantum Wells Structures

This section show the parameters and the simulation results of the superlattices of quantum wells structures obtained in the optimization process.
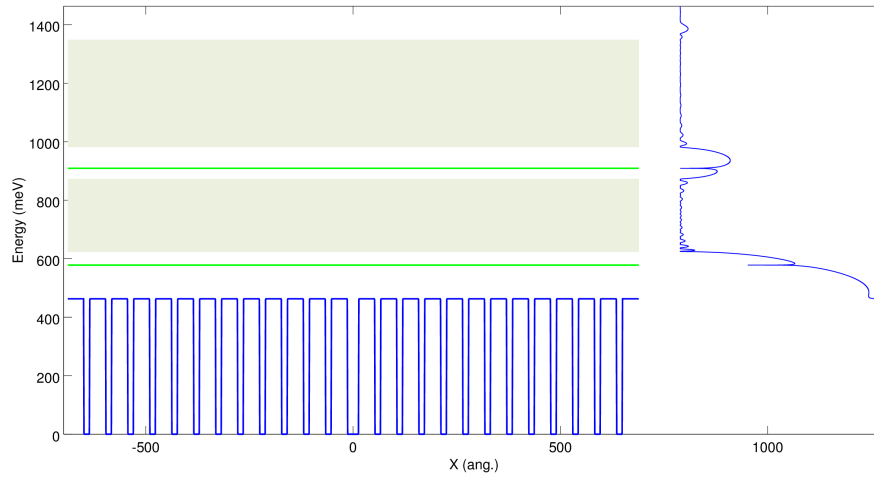
- Superlattice of quantum wells structure 1.

Number of Quantum Wells	12
Central Quantum Well Width	27 Ang.
Superlattices of Quantum Wells Width	14 Ang.
Barriers Width	39 Ang.
Barriers Height	463 meV

Table C.1: Parameter of superlattice of quantum wells structure 1.

Energy Value	Localizated State
578.22	Discrete Energy Level
624.90	Beginning of Miniband
871.70	End of Miniband
909.07	Discrete Energy Level
983.13	Beginning of Miniband
1347.09	End of Miniband

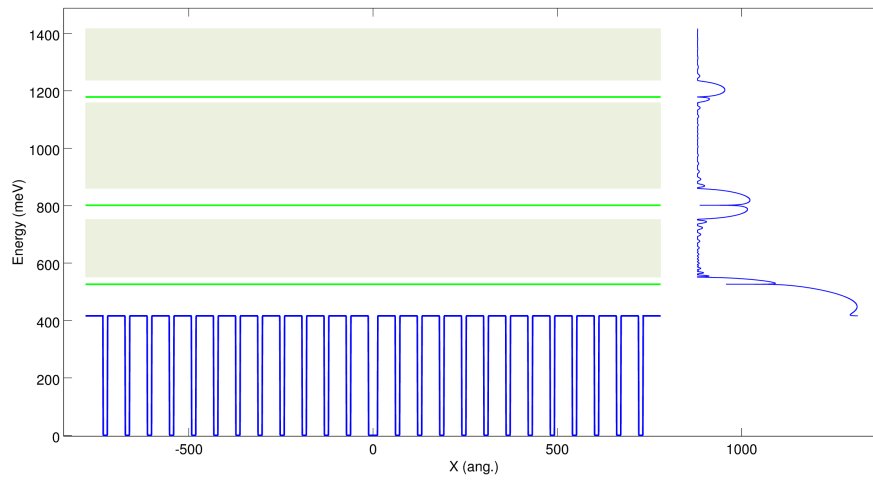Table C.2: Energy localization of structure 1.

- Superlattice of quantum wells structure 2.

Number of Quantum Wells	12
Central Quantum Well Width	25 Ang.
Superlattices of Quantum Wells Width	12 Ang.
Barriers Width	48 Ang.
Barriers Height	416 meV

Table C.3: Parameter of superlattice of quantum wells structure 2.

Energy Value	Localizated State
526.18	Discrete Energy Level
550.99	Beginning of Miniband
751.79	End of Miniband
801.24	Discrete Energy Level
860.49	Beginning of Miniband
1157.18	End of Miniband
1178.32	Discrete Energy Level
1237.60	Beginning of Miniband
1416	End of Miniband

Table C.4: Energy localization of structure 2.

- Superlattice of quantum wells structure 3.

Number of Quantum Wells	12
Central Quantum Well Width	46 Ang.
Superlattices of Quantum Wells Width	16 Ang.
Barriers Width	43 Ang.
Barriers Height	531 meV

Table C.5: Parameter of superlattice of quantum wells structure 3.

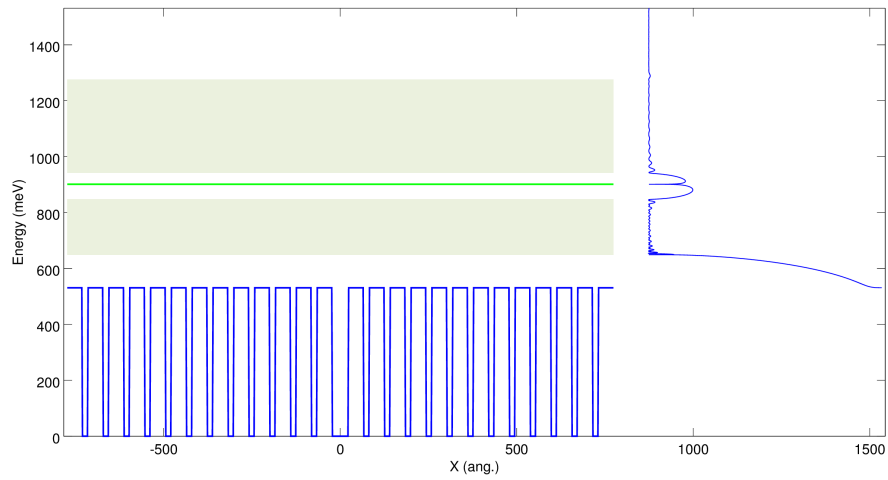| Energy Value	Localizated State
649.35	Beginning of Miniband
846.47	End of Miniband
901.38	Discrete Energy Level
943.18	Beginning of Miniband
1275.82	End of Miniband

Table C.6: Energy localization of structure 3.

Figure C.1: Superlattice of quantum wells structure 3.

- Superlattice of quantum wells structure 4.

Number of Quantum Wells	13
Central Quantum Well Width	34 Ang.
Superlattices of Quantum Wells Width	21 Ang.
Barriers Width	43 Ang.
Barriers Height	485 meV

Table C.7: Parameter of superlattice of quantum wells structure 4.

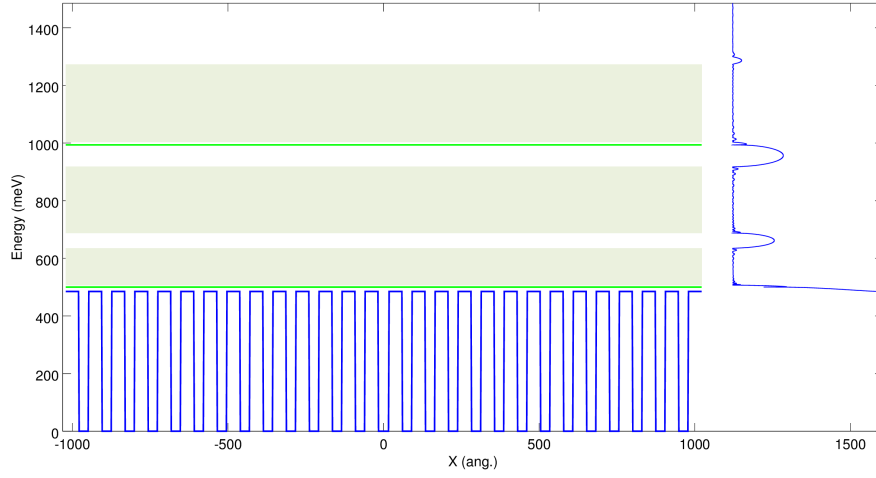| Energy Value	Localizated State
500.24	Discrete Energy Level
507.13	Beginning of Miniband
634.24	End of Miniband
687.88	Beginning of Miniband
917.03	End of Miniband
993.52	Discrete Energy Level
1003.86	Beginning of Miniband
1272.22	End of Miniband

Table C.8: Energy localization of structure 4.

Figure C.2: Superlattice of quantum wells structure 4.

- Superlattice of quantum wells structure 5.

Number of Quantum Wells	7
Central Quantum Well Width	63 Ang.
Superlattices of Quantum Wells Width	16 Ang.
Barriers Width	48 Ang.
Barriers Height	501 meV

Table C.9: Parameter of superlattice of quantum wells structure 5.

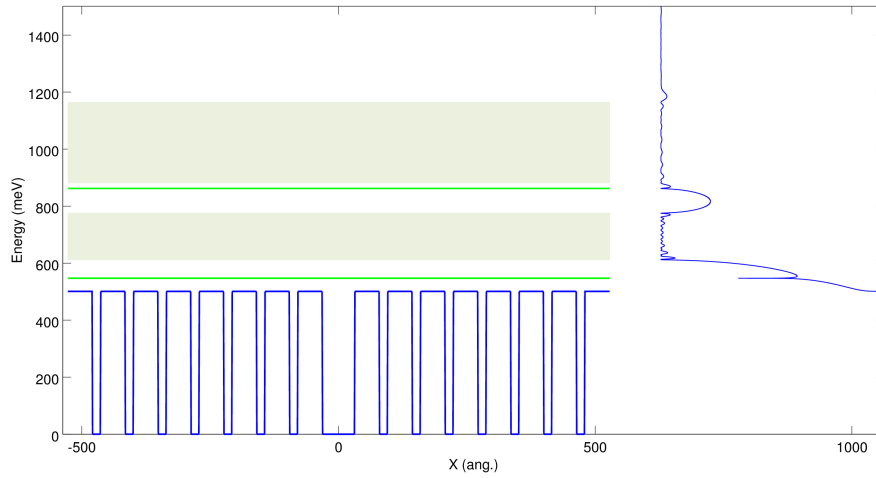| Energy Value	Localizated State
547.12	Discrete Energy Level
612.23	Beginning of Miniband
774.97	End of Miniband
862.08	Discrete Energy Level
881.65	Beginning of Miniband
1163.71	End of Miniband

Table C.10: Energy localization of structure 5.

Figure C.3: Superlattice of quantum wells structure 5.

• Superlattice of quantum wells structure 6.

Number of Quantum Wells	14
Central Quantum Well Width	62 Ang.
Superlattices of Quantum Wells Width	18 Ang.
Barriers Width	55 Ang.
Barriers Height	413 meV

Table C.11: Parameter of superlattice of quantum wells structure 6.

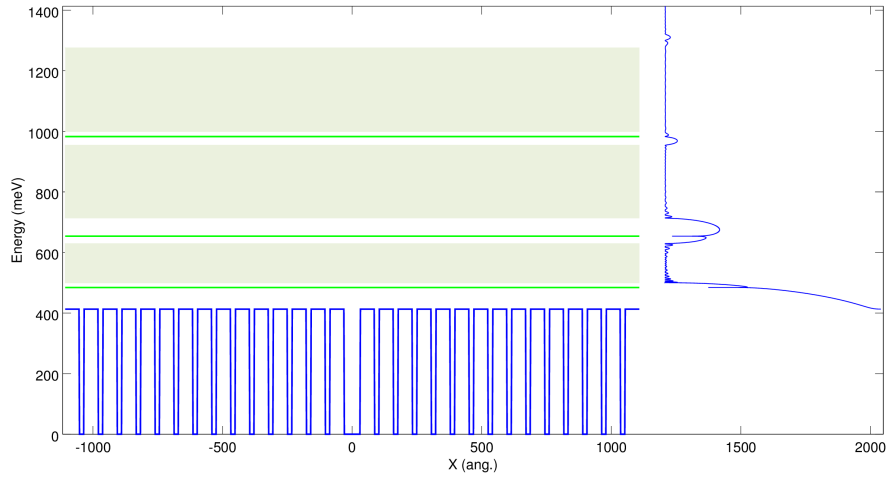| Energy Value	Localizated State
484.34	Discrete Energy Level
500.37	Beginning of Miniband
629.26	End of Miniband
653.94	Discrete Energy Level
714.00	Beginning of Miniband
953.58	End of Miniband
982.89	Discrete Energy Level
999.78	Beginning of Miniband
1275.57	End of Miniband

Table C.12: Energy localization of structure 6.

Figure C.4: Superlattice of quantum wells structure 6.

• Superlattice of quantum wells structure 7.

Number of Quantum Wells	8
Central Quantum Well Width	62 Ang.
Superlattices of Quantum Wells Width	16 Ang.
Barriers Width	51 Ang.
Barriers Height	495 meV

Table C.13: Parameter of superlattice of quantum wells structure 7.

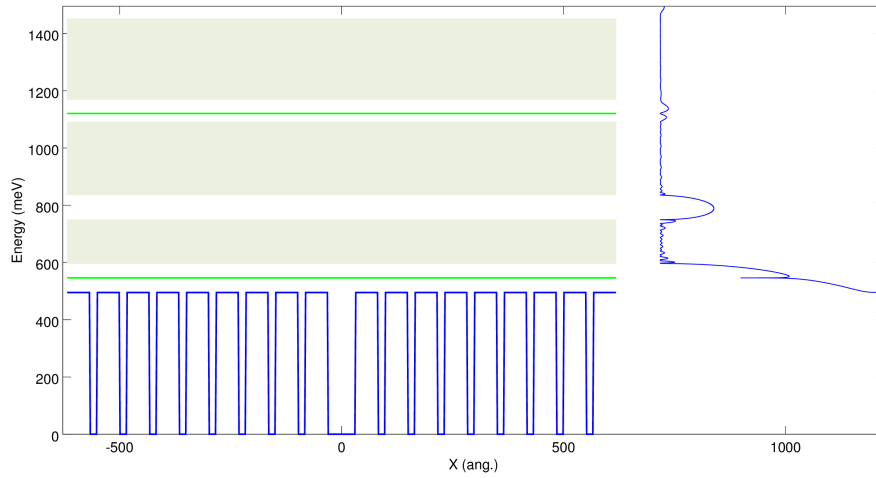| Energy Value	Localizated State
546.084	Discrete Energy Level
596.99	Beginning of Miniband
749.32	End of Miniband
835.74	Beginning of Miniband
1090.00	End of Miniband
1120.40	Discrete Energy Level
1170.32	Beginning of Miniband
1451.00	End of Miniband

Table C.14: Energy localization of structure 7.

Figure C.5: Superlattice of quantum wells structure 7.

- Superlattice of quantum wells structure 8.

Number of Quantum Wells	8
Central Quantum Well Width	63 Ang.
Superlattices of Quantum Wells Width	16 Ang.
Barriers Width	47 Ang.
Barriers Height	504 meV

Table C.15: Parameter of superlattice of quantum wells structure 8.

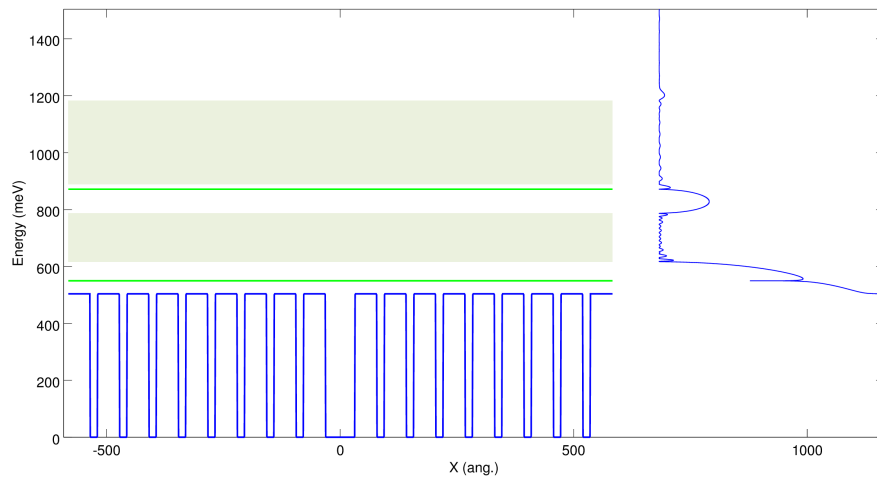| Energy Value	Localizated State
549.75	Discrete Energy Level
617.21	Beginning of Miniband
786.64	End of Miniband
871.66	Discrete Energy Level
889.95	Beginning of Miniband
1182.64	End of Miniband

Table C.16: Energy localization of structure 8.

Figure C.6: Superlattice of quantum wells structure 8.